

Magnetic field fluctuation properties of coronal mass ejection-driven sheath regions in the near-Earth solar wind

Emilia K. J. Kilpua¹, Dominique Fontaine², Simon W. Good¹, Matti Ala-Lahti¹, Adnane Osmane¹, Erika Palmerio^{1,3}, Emiliya Yordanova⁴, Clement Moissard², Lina Z. Hadid^{4,5}, and Miho Janvier⁶

¹Department of Physics, University of Helsinki, Helsinki, Finland

²LPP, CNRS, Ecole Polytechnique, Sorbonne Université, Université Paris-Saclay, Observatoire de Paris, Institut Polytechnique de Paris, PSL Research University, Palaiseau, France

³Space Sciences Laboratory, University of California–Berkeley, Berkeley, CA, USA

⁴Swedish Institute of Space Physics, Uppsala, Sweden

⁵ESTEC, European Space Agency, Noordwijk, Netherlands

⁶Institut d’Astrophysique Spatiale, CNRS, Université Paris-Sud, Université Paris-Saclay, Orsay, France

Correspondence to: Emilia Kilpua (emilia.kilpua@helsinki.fi)

Abstract. In this work, we investigate magnetic field fluctuations in three coronal mass ejection (CME)-driven sheath regions at 1 AU with their speeds ranging from slow to fast. The data set we use consists primarily of high-resolution (0.092 s) magnetic field measurements from the Wind spacecraft. We analyse magnetic field fluctuation amplitudes, compressibility, and spectral properties of fluctuations. We also analyse intermittency using various approaches: we apply the partial variance of increments (PVI) method, investigate probability distribution functions of fluctuations, including their skewness and kurtosis, and perform a structure function analysis. Our analysis is conducted separately for three different subregions within the sheath and one in the solar wind ahead of it, each 1 hr in duration. We find that, for all cases, the transition from the solar wind ahead to the sheath generates new fluctuations and the intermittency and compressibility increase, while the region closest to the ejecta leading edge resembled the solar wind ahead. The spectral indices exhibit large variability in different parts of the sheath, but are typically steeper than Kolmogorov’s in the inertial range. **The structure function analysis produced generally the best fit with the extended p -model, suggesting that turbulence is not fully developed in CME sheaths near Earth’s orbit. Both Kraichnan–Iroshnikov and Kolmogorov’s forms yielded high intermittency but different spectral slopes, questioning how well these models can describe turbulence in sheaths.** At the smallest timescales investigated, the spectral indices indicate relatively shallower than the expected slope in the dissipation range (between -2 and -2.5), suggesting that in CME-driven sheaths at 1 AU the energy cascade from larger to smaller scales could still be ongoing through the ion scale. Many turbulent properties of sheaths (e.g., spectral indices and compressibility) resemble those of the slow wind, rather than the fast one. They are also partly similar to properties reported in terrestrial magnetosheath, in particular regarding their intermittency, compressibility, and absence of Kolmogorov’s type turbulence. Our study also reveals that turbulent properties can vary considerably within the sheath. This was in particular the case for the fast sheath behind the strong and quasi-parallel shock, including a small, coherent structure embedded close to its midpoint. Our results support the view of the complex formation of the sheath and different physical mechanisms playing a role in generating fluctuations in them.

Keywords. Coronal mass ejections, Space plasma physics, Solar wind

1 Introduction

Coronal mass ejection (CME)-driven sheath regions (e.g., Kilpua et al., 2017a) are turbulent large-scale heliospheric structures that are important drivers of disturbances in the near-Earth environment and present a useful natural laboratory to study many
5 fundamental plasma physical phenomena. Sheaths form gradually as the CME travels through the solar wind from the Sun to Earth and they feature properties of both expansion and propagation sheaths (e.g., Siscoe and Odstrcil, 2008). As sheaths accumulate from layers of inhomogeneous plasma and magnetic field ahead, discontinuities and reconnection exhausts can be commonly found (e.g., Feng and Wang, 2013). Magnetic field fluctuations in the sheaths are both transmitted from the preceding solar wind and generated within the sheath, e.g., via physical processes at the shock and due to draping of the
10 magnetic field around the driving ejecta (e.g., Gosling and McComas, 1987; Kataoka et al., 2005; Siscoe et al., 2007). Sheaths also embed various plasma waves; for instance, mirror mode and Alfvén ion cyclotron waves are frequently found (Ala-Lahti et al., 2018, 2019). The compressed and turbulent nature of the sheaths enhances solar wind–magnetosphere coupling efficiency when they interact with Earth’s magnetic environment (Kilpua et al., 2017b). Sheaths have indeed been shown to be important drivers of geomagnetic storms (e.g., Tsurutani et al., 1988; Huttunen et al., 2002; Zhang et al., 2007; Echer et al., 2008;
15 Yermolaev et al., 2010); in particular, they often cause intense responses in the high-latitude magnetosphere and ionosphere (e.g., Huttunen and Koskinen, 2004; Nikolaeva et al., 2011), they are related to intense and diverse wave activity in the inner magnetosphere (e.g., Kilpua et al., 2019b; Kalliokoski et al., 2020), and produce drastic variations in high-energy electron fluxes in the Van Allen radiation belts (e.g., Hietala et al., 2014; Kilpua et al., 2015; Lugaz et al., 2015; Alves et al., 2016; Turner et al., 2019).

20 Despite their importance for heliophysics and solar–terrestrial studies, CME-driven sheath regions are currently relatively little investigated and their multi-scale structure is not well understood. In particular, a better understanding of the nature and properties of the magnetic field fluctuations in sheaths and how these properties vary spatially within them are crucial for understanding their formation and space weather impact. Detailed studies of magnetic field fluctuations in sheaths are also expected to yield new insight into outstanding problems in turbulence research, such as how intermittency in turbulence is
25 related to the formation of coherent structures and discontinuities (e.g., current sheets) in plasmas.

Good et al. (2020) investigated the radial evolution of magnetic field fluctuations for a CME-driven sheath using almost radially aligned observations made by MESSENGER at ~ 0.5 AU and STEREO-B at ~ 1 AU. At ~ 0.5 AU, where the leading-edge shock was quasi-parallel, the downstream sheath plasma developed a range of large-angle field rotations, discontinuities and complex structure that were absent in the upstream wind, with a corresponding steepening of the inertial-range spectral
30 slope and increase in mean fluctuation compressibility in the sheath. At ~ 1 AU, in contrast, the shock crossing was quasi-perpendicular and much less difference in fluctuation properties between the sheath plasma and upstream wind was observed. Intermittency in the sheath turbulence grew between the spacecraft. The shock–sheath transition at MESSENGER had a qualitatively similar ‘ageing’ effect on the plasma to that seen in the ambient solar wind with radial propagation between the

two spacecraft. Moissard et al. (2019) performed a statistical investigation of magnetic field fluctuations in 42 CME-driven sheath regions observed in the near-Earth solar wind. In particular, the authors studied compressibility $C = P_{\parallel}/(P_{\perp} + P_{\parallel})$ and anisotropy $A = P_{\perp}/(2P_{\parallel})$, where P_{\parallel} and P_{\perp} are the parallel and perpendicular power of fluctuations, respectively. They found that sheaths present increased compressibility and lower anisotropy when compared to the preceding solar wind or to
5 the following CME ejecta. The total fluctuation power was also considerably (~ 10 times) higher in the sheath than in the surrounding solar wind, consistent with some earlier studies (e.g., Kilpua et al., 2013). The fluctuation power was also found to be predominantly in the direction perpendicular to the magnetic field.

Properties of the driving CME and preceding solar wind are likely to have a significant role for turbulence in sheaths. Kilpua et al. (2013) and Kilpua et al. (2019a) reported an increase in magnetic field fluctuation power with increasing CME speed.
10 Moissard et al. (2019) found this same tendency and also emphasised the importance of the magnetic field fluctuation power in the preceding solar wind. **A clear dependence of the inertial (magnetohydrodynamic) range spectra of the ion flux fluctuations on the large solar wind driver were found by Riazantseva et al. (2019) using high-resolution SPEKTR-R plasma data and Wind magnetic field data. They separated drivers into fast and slow solar wind, magnetic clouds and non-cloud ejecta, sheaths and fast–slow stream interaction regions (SIRs; e.g., Richardson, 2018). They found, e.g., that**
15 **the inertial (magnetohydrodynamic) range spectral slopes in the slow solar wind, in sheaths ahead of non-cloud ejecta, and within magnetic clouds were less steep than the $f^{-5/3}$ power law for Kolmogorov turbulence, while the slopes in the fast solar wind, in sheaths ahead of magnetic clouds, and within ejecta were closer to the Kolmogorov index. In the kinetic range, in turn, fluctuation spectra were steepest in compressive heliospheric structures, i.e. in sheaths and SIRs.**

In this work, we analyse three CME-driven sheath regions in the near-Earth solar wind that present high, intermediate, and
20 low speeds. The Mach numbers of the shocks preceding these sheaths range correspondingly from high (4.9) to low (1.8) and their shock angles from quasi-parallel (33°) to almost perpendicular (86°). We investigate and compare distributions of the embedded magnetic field fluctuations, fluctuation amplitudes normalised to the mean magnetic field, compressibility, and intermittency. Our study is conducted for three separate 1-hour periods within the sheaths: near the shock, in the middle of the sheath, and close to the ejecta leading edge. This division is applied because properties in sheath regions often change
25 considerably from the shock to the ejecta leading edge and magnetic field fluctuations in different parts can partly arise from different physical processes (e.g., Kilpua et al., 2019b). We also include in the study one hour of the preceding solar wind for each event and investigate how fluctuation properties change from the solar wind to the sheath.

The manuscript is organised as follows: In Section 2 we describe the data sets used and some underlying assumptions. In Section 3 we present our analysis. First, we give a general overview of the three sheath events under study. Then, we investigate
30 the properties of magnetic field fluctuations, spectral indices, and compressibility. Finally, we explore the intermittency of fluctuations in more detail by analysing distribution functions, skewness, kurtosis, and structure functions. In Section 4 we discuss and in Section 5 we summarise our results.

2 Research data and assumptions

We primarily use high-resolution magnetic field observations from the Magnetic Fields Investigation (MFI; Lepping et al., 1995) instrument on board the Wind (Ogilvie and Desch, 1997) spacecraft. The magnetic field data during the observed events are available at 0.092-s cadence. We obtained the data through the NASA Goddard Space Flight Center Coordinated Data Analysis Web¹ (CDAWeb). To provide an overview of the wider solar wind conditions for the studied events, we also used plasma data from Wind’s Solar Wind Experiment (SWE; Ogilvie et al., 1995) instrument, which are available at 90-s resolution. During the times of the events that are part of this study, Wind was located at the Lagrange L1 point.

In our analysis, we divide sheaths into three separate regions, each being one hour in duration. Furthermore, we consider a one-hour region of solar wind preceding the shock and sheath, excluding the 30-min period immediately ahead of the shock. The three distinct regions within the sheath are termed the Near-Shock, Mid-Sheath, and Near-Leading Edge (Near-LE) regions. The Near-Shock region extends from the shock to the sheath, excluding the 15 minutes immediately following the shock, and the Near-LE region ends 15 minutes before the leading edge of the ICME ejecta. The 15-min interval closest to the shock and the ejecta leading edge have been excluded to avoid the shock transitions and most immediate shock processes and uncertainties in the timing of the ejecta leading edge, respectively. The Mid-Sheath regions are located around the middle of the sheath, except for the fast event for which the Mid-Sheath region was selected to capture a coherent magnetic field structure embedded in the sheath. We however emphasise that the results for the Mid-Sheath are likely to depend strongly on the selected interval.

The fluctuations in the magnetic field are defined here as $\delta\mathbf{B} = \mathbf{B}(t) - \mathbf{B}(t + \Delta t)$, and fluctuation amplitude $\delta B = |\delta\mathbf{B}|$, where Δt is the timescale or time-lag between two samples. We use 14 values of Δt that range from 0.092 to 736 s (12.3 min), where the values are successively doubled. The observations thus cover most of the inertial range ($10^1 \text{ s} \lesssim \Delta t \lesssim 10^3 \text{ s}$) and the upper part of the sub-ion (kinetic) range ($\Delta t \lesssim 10^1 \text{ s}$).

We study magnetic field fluctuations in the spacecraft frame, which is in relative motion with respect to the solar wind frame. To justify the transformation from spacecraft frequency to wavenumber, and to relate observed timescales to length scales in the plasma, the so-called Taylor hypothesis (Taylor, 1938; Matthaeus and Goldstein, 1982) must be valid. The hypothesis states in this context that when the timescales of the magnetic field fluctuations are much less than the timescale of rapidly flowing solar wind, the path of a spacecraft travelling through solar wind represents an instantaneous spatial cut. This can be expressed in a simple way as $\kappa = v_A/v \lesssim 1$ (Howes et al., 2014), where v_A is the Alfvén speed, and v the solar wind speed. The results are shown in Table 1, where it can be seen that for all events and subregions the criterion is met in this study.

3 Analysis and results

3.1 Event overview

We analyse three CME-driven sheath regions detected by the Wind spacecraft in the near-Earth solar wind at the Lagrange L1 point. The key parameters of these events are listed in Table 1. The events were selected from the list of 81 sheaths published

¹<http://cdaweb.gsfc.nasa.gov/>

Table 1. Summary of the events analysed. The first two rows give the shock and CME ejecta leading edge (LE) times at Wind. The following rows give the shock parameters: magnetosonic Mach number (M_{ms}), shock angle (θ_{Bn} , i.e., the angle between the shock normal and upstream magnetic field), shock speed (V_{shock}), and upstream plasma beta (β_u). The next rows give the sheath parameters: the duration of the sheath (ΔT), the average solar wind speed in the sheath ($\langle V_{sheath} \rangle$), the average magnetic field magnitude ($\langle B_{sheath} \rangle$), the parameter κ , defined as $\kappa = v_A/v$ and that tests the validity of the Taylor hypothesis (see Section 2 for details), and the ‘PMS coverage’, which indicates the percentage of the sheath subregions occupied by planar magnetic structure (PMS)-type field behaviour (see Section 3.1). The last rows give the average solar wind speed and κ values for the one-hour solar wind interval preceding the shock.

| | Dec 14, 2006 (Fast) | Oct 24, 2001 (Medium speed) | Oct 31, 2012 (Slow) |
|-------------------------------------|---------------------|-----------------------------|---------------------|
| Time | | | |
| Shock [UT] | 12/14/2006 13:51 | 10/24/2011 17:39 | 10/31/2012 14:28 |
| Ejecta LE [UT] | 12/14/2006 22:36 | 10/25/2011 00:21 | 10/31/2012 23:30 |
| Shock | | | |
| M_{ms} | 4.9 | 2.5 | 1.8 |
| θ_{Bn} [°] | 33 | 64 | 86 |
| V_{shock} [km/s] | 919 | 542 | 391 |
| β_u | 5.2 | 1.4 | 5.2 |
| Sheath | | | |
| ΔT [hours] | 8.7 | 6.9 | 9.0 |
| $\langle V_{sheath} \rangle$ [km/s] | 880 | 503 | 351 |
| $\langle B_{sheath} \rangle$ [nT] | 11.5 | 15.5 | 9.4 |
| κ | 0.11–0.11–0.07 | 0.15–0.11–0.16 | 0.09–0.13–0.14 |
| PMS coverage | 0%–100%–100% | 100%–0%–0% | 0%–100%–100% |
| Preceding solar wind | | | |
| $\langle V_{sw} \rangle$ [km/s] | 584 | 340 | 290 |
| κ | 0.12 | 0.13 | 0.12 |

in Kilpua et al. (2019b) to have their speeds to represent the lowest, median, and highest speeds of the whole population. The speed of the sheath was selected as our primary parameter for the event selection since solar wind turbulence studies often consider slow and fast wind separately due to their different evolution and origin, which affects their turbulent properties. We also required that the selected sheaths had at least 4 hours in duration, were followed by a well-defined CME ejecta that was classified as a magnetic cloud in the Richardson and Cane ICME list² (Richardson and Cane, 2010), presented a clear transition from the sheath to the ejecta, and that no other CMEs were present within a one-day period prior to the interplanetary shock ahead of the sheath. The selected events are: December 14–15, 2006 (fast sheath), October 24–25, 2011 (medium-speed sheath), and October 31, 2012 (slow sheath) with their mean speeds calculated over the duration of the whole sheath being 880, 503, and 351 km/s, respectively. Table 1 also shows that the investigated events have also different shock strengths and shock speeds. The fast sheath was preceded by the strongest and fastest shock (4.9 and 919 km/s), while the slow event was preceded by the weakest and slowest shock (1.8 and 391 km/s). The shock angles (θ_{Bn} , i.e., the angle between the shock normal and upstream magnetic field) were also varied amongst the events; while the fastest sheath was associated with a quasi-parallel shock (33°), the intermediate and slow sheaths were preceded by quasi-perpendicular shocks. For the slowest sheath the shock angle was very close the perpendicular ($\theta_{Bn} = 86^\circ$) The shock configuration is also expected to affect magnetic field fluctuation properties in the sheath, in particular in the near-shock region (e.g., Bale et al., 2005a; Burgess et al., 2005).

Figure 1 shows the solar wind conditions during the three events under study. The orange-shaded intervals show the one-hour regions subject to a more detailed analysis. The first four panels give the interplanetary magnetic field (IMF) magnitude, IMF components in GSE coordinates (blue: B_X , green: B_Y , red: B_Z), solar wind speed, and density. It is clear that all three cases present well-defined sheath regions with large-amplitude magnetic field fluctuations embedded, and enhanced solar wind density. It is however evident that the overall properties of the sheath vary considerable between the three events and from the shock to ejecta leading edge. We also note that the fast sheath is preceded by fast solar wind, while the medium-speed and slow sheaths are preceded by slow wind. **The largest fluctuations seem to be associated with the north-south magnetic field component (B_Z).**

The last panel of Figure 1 gives the normalised partial variance of increments (PVI). The PVI parameter is defined as

$$PVI = \frac{|\delta\mathbf{B}|}{\sqrt{\langle|\delta\mathbf{B}|^2\rangle}}, \quad (1)$$

where the average in the denominator is taken over the whole interval shown. This quantity is used to detect coherent structures or discontinuities (e.g., Greco et al., 2018; Zhou et al., 2019). We calculate the PVI here using three different time-lags between two data points: $\Delta t = 0.18, 24, \text{ and } 186$ s (0.18 s corresponding to the kinetic range, and 24 and 186 s corresponding to the inertial range). The figure shows that the PVI exhibits a number of spikes throughout most of the sheaths investigated, suggesting that intermittent structures are frequently present. The largest PVI spikes in the fast and medium-speed sheath occur close to the shock, while for the slow sheath they are found close to the middle part of the sheath. The coherent structure in fast sheath exhibits low PVI. Another interesting feature visible from the PVI panel is that the Near-LE regions, in particular

²<http://www.srl.caltech.edu/ACE/ASC/DATA/level3/icmetable2.htm>

for the medium-speed and slow sheaths, have similar PVI levels as the solar wind ahead of them (excluding the peaks at the sheath-ejecta transition).

Table 1 shows the percentage of the sheath subregions occupied by planar magnetic structures (PMSs) determined with the method described in Palmerio et al. (2016). PMSs are periods during which the variations of the magnetic field vectors remain nearly parallel to a fixed plane over an extended time period (e.g., Nakagawa et al., 1989; Jones and Balogh, 2000). PMSs typically cover a significant part of the sheath and can be present in all parts of the sheath (Palmerio et al., 2016). In CME-driven sheaths, they are thought to arise from processes at the shock (i.e. the alignment and amplification of pre-existing discontinuities; e.g. Neugebauer et al., 1993; Kataoka et al., 2005) and field-line draping around the CME ejecta (e.g., Gosling and McComas, 1987). As reported by Kataoka et al. (2005) and Palmerio et al. (2016), PMSs are most frequently found behind strong quasi-perpendicular shocks with high upstream plasma beta. The fast sheath and the slow one had no PMS in their Near-Shock region, but their Mid-Sheath and Near-LE regions were fully covered by planar fields. The lack of PMSs in the Near-Shock region for the fast sheath is likely due to the quasi-parallel shock configuration, while for the slow sheath it is probably due to its leading shock being weak ($M_{ms} = 1.8$). The medium-speed sheath, in turn, presented planar fields in the Near-Shock region, but no PMS in the other subregions. The comparison of planar periods with the PVI values shown in Figure 1 does not reveal an obvious correlation.

3.2 Distributions and averages of magnetic field fluctuations

Figure 2 shows the Probability Distribution Functions (PDFs) of the normalised fluctuation amplitude $\delta B/B$ for timescales Δt ranging from 0.092 s (light red) to 736 s (dark red). **δB is defined in Section 2 and B is the mean magnetic field amplitude calculated over the time interval Δt . This approach is similar to, e.g., Chen et al. (2015), Matteini et al. (2018), and Good et al. (2020). These studies have indicated that in the solar wind fluctuations have dominantly small normalised fluctuation amplitudes ($\delta B/B$ values < 1), but PDFs spread to larger $\delta B/B$ values. $\delta B/B$ values exceeding $\sqrt{2}$ signify large directional changes of the field (exceeding 90°), while values > 2 indicate that fluctuations must be at least partly compressional (e.g., Chen et al., 2015). Note that for purely Alfvénic (i.e., incompressible) fluctuations the field magnitude does not change and $\delta B/B$ must be < 2 .** The columns show from left to right different subregions and from top to bottom the three different events.

The solar wind preceding the medium-speed and slow sheaths have practically all $\delta B/B$ values < 1 (left panels of Figure 2), meaning that there are no significant rotations of the field direction (no larger than 60° for pure rotation case). The fast event (Dec 14, 2006), in turn, is preceded by a solar wind with clearly larger normalised fluctuation amplitudes. The $\delta B/B$ values are nevertheless mostly < 2 , **suggesting that fluctuations are largely Alfvénic (see above).** We also note that the solar wind ahead of the fast sheath could be affected by foreshock waves, since it is ahead of the quasi-parallel shock as discussed in Section 3.1.

Comparison of the preceding solar wind and Near-Shock regions shows that the normalised fluctuation amplitudes are spread to considerably larger values in the Near-Shock region for all events and timescales investigated. This can be due to the generation of new fluctuations or amplification (in magnitude and/or change in the field direction) of pre-existing fluctuations

relative to the mean field. For the medium-speed and slow sheath distributions, $\delta B/B$ values are mostly confined to $< \sqrt{2}$ in the Near-Shock region, which means that there are no significant rotations, while for the fast sheath there is a significant fraction of values > 2 for scales $\Delta t \gtrsim 6$ s, meaning that large rotations of the field direction exist and fluctuations must be at least partly compressional.

5 Figure 2 clearly shows that the PDFs vary considerably in different sheath subregions. This is particularly evident in the fast sheath: Both the Near-Shock and Near-LE regions have PDFs extending to $\delta B/B > 2$, but for the Near-LE region this occurs for the larger time-scales only ($\Delta t \gtrsim 48$ s), i.e., at scales within the inertial range, while for the Near-Shock regions PDFs populate $\delta B/B > 2$ for $\Delta t \gtrsim 1.5$ s. Within the small coherent structure near the middle of the fast sheath, fluctuations are in turn restricted to $\delta B/B \leq 1$, thus being much smaller than in the other parts of the sheath or preceding solar wind. For the
 10 medium and slow-speed sheaths, the largest $\delta B/B$ values occur in the Mid-Sheath region and in the case of the medium-speed sheath $\delta B/B$ exceeds 2 for the largest scales.

One interesting feature in Figure 2 is that the Near-LE distributions resemble quite closely those in the solar wind ahead, both in their extent to higher $\delta B/B$ values and shape of the curves. This is most distinct for the medium-speed and slow sheaths, for which $\delta B/B$ values are mostly confined to < 1 . For the fast sheath distributions in the Near-LE region at larger
 15 scales are however clearly flatter and less smooth than in the solar wind ahead (or in the Near-Shock region).

Figure 2 also reveals the expected general trend; for the smallest timescales, PDFs have sharp peaks at low $\delta B/B$ values and then decay exponentially, while at larger timescales distributions become broader, in particular in the sheaths. This behaviour, i.e. that distributions of normalised fluctuations become more Gaussian and shift towards larger values with increasing timescale, is consistent with previous studies carried out in the solar wind (e.g., Sorriso-Valvo et al., 2001; Chen et al., 2015;
 20 Matteini et al., 2018). **We will return to investigate this in more detail in Section 3.5.1.**

We now consider the average fluctuation amplitudes across the range of timescales. The top and middle panels of Figure 3 show the mean values of δB and $\delta B/B$ as a function of timescale. **In the top panel, the ion cyclotron timescales (t_{ci}) are also plotted, using the mean magnetic field magnitude over the whole subregion in question. t_{ci} is obtained as an inverse of ion cyclotron frequency (f_{ci}) doppler-shifted in the spacecraft frame using $f_{ci} = \frac{\langle v \rangle}{\langle v_{th} \rangle} \frac{e(B)}{2\pi m_i}$, see e.g., Chen et al. (2015).**

25 In the preceding solar wind intervals, mean fluctuation amplitudes $\langle \delta B \rangle$ and normalised fluctuation amplitudes $\langle \delta B/B \rangle$ are highest ahead of the fast sheath and lowest ahead of the slow sheath. We however note that differences are partly relatively small, in particular for the mean fluctuation amplitudes between the fast and medium-speed sheath. As is to be expected considering the field compression at the shock, $\langle \delta B \rangle$ are considerably higher in the Near-Shock region than in the preceding solar wind for all events and timescales. The $\langle \delta B/B \rangle$ are also higher in the Near-Shock and Mid-Sheath regions than in the
 30 solar wind ahead, also reported in Good et al. (2020). This suggests that the transition from the solar wind to the sheath generates new and/or enhances pre-existing magnetic field fluctuations at all timescales.

Matteini et al. (2018) reported that the spectra of normalised fluctuation amplitudes collapsed on the same curve for the solar wind periods observed by Helios and Ulysses, suggesting the modulation of the field fluctuations with the magnetic field magnitude. Their results were however obtained at varying heliospheric distances and solar wind speeds. In our study $\langle \delta B \rangle$
 35 curves are organised according to the solar wind speed as mentioned above. This trending is maintained throughout the sheath,

except for the small coherent structure in the mid-point of the fast sheath that exhibits both lower $\langle \delta B \rangle$ and $\langle \delta B/B \rangle$ values (especially so at larger scales) than in the solar wind ahead or in the Mid-Sheath regions of the other two sheaths.

3.3 Spectral indices

Several studies have investigated how the power spectrum of solar wind magnetic field fluctuations is in agreement with predic-
5 tions made by turbulence theories (e.g., Coleman, 1968; Bavassano et al., 1982; Horbury and Balogh, 2001; Bale et al., 2005b; Tsurutani et al., 2018; Verscharen et al., 2019). Kolmogorov's spatially homogeneous hydrodynamic turbulence model gives $f^{-5/3}$ (i.e., spectral index $\alpha = -1.67$; Kolmogorov, 1941) and is based on the assumption that energy cascades from larger to smaller scales through eddies that break down evenly and are space filling. The modification of Kolmogorov's model for a magnetohydrodynamic fluid, based on works by Iroshnikov (1964) and Kraichnan (1965), takes into consideration interactions
10 between oppositely propagating Alfvén waves and equipartitioning between magnetic and kinetic energy. In the inertial regime of the Kraichnan–Iroshnikov model, the energy spectrum is proportional to $f^{-3/2}$ (i.e., spectral index $\alpha = -1.5$), i.e. less steep than in the Kolmogorov model. The energy is then dissipated in the kinetic range and the breakpoint occurs around the ion cyclotron scale ($t_{ci} = 1/f_{ci}$, where f_{ci} is the ion cyclotron frequency). The kinetic regime exhibits a steeper spectral slope than the inertial regime, with spectral index $\alpha_k \simeq -2.8$ typically reported in the solar wind (e.g., Alexandrova et al., 2013; Bruno et al., 2017; Huang et al., 2017). The timescales studied here should generally be below the energy-driving f^{-1} regime, which occurs at frequencies $f \gtrsim 10^{-3}$ Hz for the fast wind, i.e., timescales $\gtrsim 16.7$ min (e.g., Bruno and Carbone, 2013) and at frequencies $f \gtrsim 10^{-4}$ Hz, i.e., timescales $\gtrsim 166.7$ minutes or 2.7 hours for the slow wind (e.g., Bruno, 2019). This regime known as the "energy containing scale" is likely composed of fluctuations with various origins and remains debated (see e.g. discussion in Bruno et al., 2019). We note that some of the curves in the top panels of Figure 3, in particular the preceding solar
20 wind and Near-Shock subregions in the fast sheath, exhibit a flattening trend towards the largest timescales that could indicate the transition to the f^{-1} regime. Other possibility is that, as discussed in Section 3.2, foreshock waves can affect, and could result to a small hump at timescales around 100 s.

The $\langle \delta B/B \rangle$ values in the top panels of Figure 3 can be used to calculate the slopes as their gradients are related to turbulence in the inertial range. This stems from the connection of δB^2 at scale l to k -space spectral power $P(k)$ as
25 $\delta B^2 = P(k) \cdot k$, **where $k = 1/l$ and $P(k) \approx k^\alpha$ (e.g., Matteini et al., 2018; Good et al., 2020).** The pink dashed lines $l^{0.33}$ in Figure 3 show the Kolmogorov scaling and the cyan dash-dotted lines $l^{0.25}$ the Kraichnan–Iroshnikov scaling in the inertial range. Note that the $l^{0.33}$ and $l^{0.25}$ given in the figure correspond to $\alpha = -5/3$ and $\alpha = -3/2$, respectively (e.g., Matteini et al., 2018). In the kinetic range we have plotted the scaling $l^{0.9}$ ($\alpha \simeq -2.8$). Table 2 shows the kinetic and inertial range spectral indices for the preceding solar wind and in the three subregions of the sheath. **The kinetic range indices are determined**
30 **using the first three timescales from 0.092 to 0.37 s and the inertial range indices using five timescales from 6 to 96 s.** The timescales used to calculate the inertial scale indices are above the ion cyclotron timescales for all cases and fall into the region where the $\langle \delta B \rangle$ curves have approximately a linear behaviour (see Figure 3). They are also well above the 0.3 Hz (3 s) of the dissipation range breakpoint found in the extensive statistical study at L1 by Smith et al. (2006).

Table 2. Spectral indices as calculated by fitting a straight line in log space for kinetic range ($\Delta t = 0.092\text{--}0.37$ s, three consecutive timelags) and inertial range ($\Delta t = 24\text{--}96$ s, five consecutive timelags). The values in the parenthesis show the standard deviation errors associated with the fitting. The third column gives the ion cyclotron period for each region. The last column gives $\kappa = v_A/v$ that tests the validity of the Taylor hypothesis (see Section 2 for details).

| | Kinetic | Inertial | t_{ci} [sec] | κ |
|--------------|----------------|----------------|----------------|----------|
| Fast | | | | |
| Preceding SW | −2.47 (0.0886) | −1.89 (0.0212) | 1.28 | 0.16 |
| Near-Shock | −2.49 (0.0128) | −1.74 (0.0292) | 0.87 | 0.17 |
| Mid-Sheath | −2.23 (0.0972) | −1.54 (0.0212) | 0.53 | 0.21 |
| Near-LE | −2.27 (0.0140) | −1.91 (0.0421) | 0.28 | 0.18 |
| Intermediate | | | | |
| Preceding SW | −2.29 (0.0986) | −1.58 (0.0302) | 1.25 | 0.16 |
| Near-Shock | −2.41 (0.0850) | −1.70 (0.0449) | 0.62 | 0.28 |
| Mid-Sheath | −2.42 (0.0222) | −1.90 (0.0399) | 0.72 | 0.18 |
| Near-LE | −2.44 (0.0102) | −1.57 (0.0306) | 0.28 | 0.21 |
| Slow | | | | |
| Preceding SW | −1.72 (0.0329) | −1.65 (0.0226) | 0.93 | 0.12 |
| Near-Shock | −2.37 (0.0129) | −1.77 (0.0691) | 0.77 | 0.15 |
| Mid-Sheath | −2.56 (0.0914) | −1.76 (0.0190) | 0.75 | 0.17 |
| Near-LE | −2.15 (0.0624) | −1.71 (0.0240) | 0.80 | 0.28 |

In the kinetic range, the spectral slopes are consistently less steep than the -2.8 index cited above. For the solar wind preceding the slow sheath, the kinetic range spectral index is -1.72 , while in other regions they are distributed between -2.23 and -2.49 . In the inertial range the spectral indices vary considerably. The Near-Shock region for the fast sheath, Near-Shock and Near-LE regions for the medium-speed sheath, and the preceding solar wind region for the slow sheath have their inertial range spectral indices matching or close to the Kolmogorov index (-1.67). The Mid-Sheath region for the fast sheath and the preceding solar wind for the medium-speed sheath exhibit in turn their spectral index close to the Kraichnan–Iroshnikov value (-1.5). Otherwise, the spectral indices are clearly steeper than Kolmogorov’s. For the fast sheath, the slope in the preceding solar wind region could have been affected by the possible foreshock wave related hump (see above) and the slope could be in reality closer to Kolmogorov’s.

10 3.4 Compressibility

The bottom panels of Figure 3 show the mean of $\delta|B|/\delta B$. This parameter gives the compressibility of magnetic fluctuations, i.e. the mean amount of compression as a fraction of the total fluctuation amplitude, as a function of timescale. The horizontal

line is at $\delta|B|/\delta B = 0.2$ (Matteini et al., 2018), which represents the typical upper threshold of the level of compressibility in magnetic field fluctuations found for the fast solar wind in the inertial regime; the slow solar wind tends to have $\delta|B|/\delta B$ values exceeding 0.2.

For all cases investigated, compressibility increases from the solar wind ahead to the Near-Shock region, suggesting that the locally-generated new fluctuations in the sheath are at least partly compressible. This occurs for all timescales for the fast and slow sheaths. For the medium-speed sheath the two largest scales show a decrease, with compressibility values < 0.2 . Again, it is possible that this decrease at the largest scales is due to a larger statistical error, since the magnetic field magnitude does not change that much in this subregion when compared to other events. The solar wind preceding the fast sheath has $\delta|B|/\delta B$ values below 0.2 in the inertial range, consistent with its speed being in the fast-wind range (see Figure 1).

Figure 3 shows that the level of compressibility varies considerably in different subregions of the sheath. For the fast sheath, compressibility is relatively high in all sheath subregions and above the preceding solar wind values, in particular in the small coherent structure near the middle of the sheath. This is in agreement with normalized fluctuation amplitudes $\langle \delta|B|/B \rangle$ being low in the region (Section 3.2), as compressible/parallel fluctuations are known to have lower amplitudes/power than Alfvénic/perpendicular fluctuations (i.e., there is power anisotropy). For the medium speed sheath, compressibility values are also high in the Mid-Sheath, but in the Near-LE region in turn, fluctuations are even less compressible than in the preceding solar wind and for the most time-scales below 0.2. The slow sheath has most compressible fluctuations in the Near-Shock and Near-LE regions, comparable to values for the fast sheath, but in the Mid-Sheath region compressibility values fall below the preceding solar wind values and even the 0.2 threshold for the largest timescales ($\Delta t > 96$ s). In all instances, it can be seen that compressibility generally decreases from the smallest scales until about 100 s. This is a well known trend from previous solar wind studies (e.g., Chen et al., 2015; Matteini et al., 2018; Good et al., 2020). We note that the increase for the few highest timescales could be related to statistical errors in the data as discussed above.

3.5 Intermittency

Several studies have shown that fluctuations in the solar wind are typically strongly intermittent (e.g., Burlaga, 1991; Feynman and Ruzmaikin, 1994; Marsch and Tu, 1994, 1997; Pagel and Balogh, 2001; Yordanova et al., 2009). Intermittency describes inhomogeneity in the energy transfer between scales, and is manifested as a lack of self-similarity in fluctuation distributions between scales (see, e.g., reviews by Horbury et al., 2005; Sorriso-Valvo et al., 2005; Bruno, 2019; Verscharen et al., 2019). In the solar wind, it can arise from coherent structures such as current sheets and discontinuities. The PVI parameter shown in the bottom panel of Figure 1 already gives some indication that intermittent structures were embedded throughout the sheaths analysed.

3.5.1 Probability distribution functions

Deviations from a Gaussian distribution in fluctuation PDFs at different timescales can reveal the presence of intermittency. Figure 4 shows distributions of $(\delta B_Z - \mu)/\sigma$ for different Δt values. Here, σ is the standard deviation and μ the mean of δB_Z calculated using a 15-minute sliding average. The black dashed line shows the normal distribution whose standard deviation

and mean correspond that of the $(\delta B_Z - \mu)/\sigma$ distribution calculated using the 6-second timescale, but we note that normal distributions for the other shown timescales would be almost inseparable from the 6-second curve. **Similar PDFs for B_X and B_Y are shown in the Supplementary Material, Figures S1 and S2. We investigate here in detail the Z -component of the IMF since it has the largest importance for the solar wind magnetosphere coupling and geoefficiency of the sheath.**

5 **We note that PDFs for different components are overall very similar, but B_z has somewhat heavier tails than the other components (suggesting also higher intermittency). This is consistent with Figure 1 showing the largest amplitude fluctuations for B_Z .**

The distributions in Figure 4 are clearly non-Gaussian, and particularly so at smaller timescales (light red curves) where they **are spikier** and have flatter tails: these are clear signs of intermittency. At larger timescales (dark red curves), distributions
10 become generally more Gaussian, consistent with, e.g., Greco et al. (2008). Non-self-similarity is also qualitatively evident in Figure 4.

3.5.2 Skewness and kurtosis

In order to characterise the non-Gaussian aspects of the distributions, we compute the higher-order moments. Figure 5 gives the skewness and kurtosis calculated for the distributions shown in Figure 4. Skewness is related to the third distribution
15 moment and gives information on the degree of distribution asymmetry. For the normal distribution, skewness is zero, i.e., the distribution is symmetric around the mean value. Positive skewness indicates an extended tail at larger values than the mean (i.e., weighting and a longer tail and towards the right), whereas negative skewness indicates an extended tail at smaller values than the mean (i.e., weighting and a longer tail towards the left). Kurtosis is related to the fourth distribution moment and can be used as the proxy of large fluctuations that are indication of intermittency (e.g., Krommes, 2002; Osmane et al., 2015). PDFs
20 with long tails have larger kurtosis than narrow PDFs. For the normal distribution, kurtosis is 3; values larger than 3 indicate flatter tails while values less than 3 indicate lighter tails. In Figure 5 we have subtracted the value 3 from the kurtosis, such that 0 depicts the normal distribution for both kurtosis and skewness.

For all investigated subregions skewness has mostly small absolute values (< 1), suggesting that distributions and fluctuations are generally symmetric around the mean (~ 0 nT). There are no obvious drastic differences in skewnesses between the
25 preceding solar wind and the sheath. One feature visible from the plot is that for all events the skewnesses in the preceding solar wind tend to have negative values, signifying that there is an excess of negative fluctuations, while in the sheath both negative and positive skewness values are observed more evenly. The largest absolute magnitudes of skewnesses (i.e., indicating largest asymmetries when compared to Gaussian distribution) are found for the medium-speed and slow sheaths in the Mid-Sheath region.

30 The kurtosis values are nearly all positive, indicating an excess of high-amplitude δB_Z fluctuations with respect to the normal distribution. In the majority of cases, kurtosis decreases towards zero through the inertial range, indicating that distributions become more Gaussian with increasing timescale. This is consistent with the qualitative assessment of distribution shapes discussed in Section 3.5.1. In the solar wind, kurtosis peaks broadly near the small-scale end of the inertial range, and reduces in value with decreasing scale through the kinetic range (most clear for the medium-speed and slow event). Across the same

scales in the sheaths, in contrast, kurtosis flattens or continues to increase with reducing scale. Peaks in kurtosis are associated with the inertial–kinetic spectral breakpoint (e.g., Chen et al., 2015); the ion cyclotron period (Table 1), which is in the vicinity of this spectral break, is larger in the preceding solar wind than in the sheaths, which may partly explain the more obvious kurtosis peaks. There is also a clear general increase in kurtosis between the solar wind ahead and Near-LE regions for the 5 slow and intermediate speed events, while there is no significant change in values for the fast event. This could indicate that the Near-LE distributions are less peaked for the fast sheath, i.e. in contrast to the behaviour of the medium-speed and slow sheaths.

3.5.3 Structure function analysis

Intermittency can be also investigated using structure functions (e.g., Bruno and Carbone, 2013). The structure function of 10 order m of the fluctuation amplitude in the i th magnetic field component is

$$S_{B,i}^m(\Delta t) = \langle |\delta B_i| \rangle = \langle |B_i(t) - B_i(\Delta t + t)|^m \rangle. \quad (2)$$

If the system conforms to a self-similar scaling law, then $S_B^m(\Delta t) \sim \Delta t^{g(m)}$. The scaling exponent is $g(m) = m/3$ (i.e., $S_B^m(\Delta t) \sim \Delta t^{m/3}$) in Kolmogorov’s turbulence and $g(m) = m/4$ in the Kraichnan–Iroshnikov model.

To account for intermittency and inhomogenities in the energy transfer between scales, various turbulence models have 15 been proposed in the literature (see a more detailed description from e.g. Horbury and Balogh, 1997; Bruno, 2019). Several models have been shown to fit observations reasonably well; for brevity, only results for the p -model are shown here. We note that other models were tested, e.g. the random β -model (Frisch et al., 1978; Paladin and Vulpiani, 1987) and the She–Levyque model (She and Leveque, 1994), but it was found that the p -model agreed best with the observed structure function scaling.

The standard p -model by Meneveau and Sreenivasan (1987) (see also Tu et al., 1996) assumes fully-developed turbulence 20 in which intermittency arises from the unequal breakdown of eddies, i.e., resulting daughter eddies have different amount of energy. The structure function scaling exponents in the p -model are defined as

$$g(m) = 1 - \log_2[p^{m/q} + (1-p)^{m/q}], \quad (3)$$

where the intermittency parameter p varies between 0.5 and 1. The parameter q is 3 in the Kolmogorov form and 4 for 25 the Kraichnan–Iroshnikov form (e.g., Carbone, 1993). The p value of 0.5 corresponds to the non-intermittent case, giving $g(m) = m/3$ for Kolmogorov and $g(m) = m/4$ for Kraichnan–Iroshnikov turbulence. In the non-intermittent case, the structure function scaling exponents are linear with the moment m . Where there is intermittency, the scaling exponents flatten for larger m and curves become nonlinear. The maximum intermittency in both cases occurs for $p = 1$, i.e. $g(m) = 1$.

The extended p -model(Tu et al., 1996; Marsch and Tu, 1997) describes turbulence that is not fully developed, as has been identified, for example, in the inner heliosphere. In the Kolmogorov form,

$$30 \quad g(m) = \left(-\frac{5}{3} + \frac{3}{2}\alpha'\right)\frac{m}{3} + 1 - \log_2[p^{m/3} + (1-p)^{m/3}], \quad (4)$$

and in the Kraichnan–Iroshnikov form,

$$g(m) = (-3 + 2\alpha')\frac{m}{4} + 1 - \log_2[p^{m/4} + (1-p)^{m/4}]. \quad (5)$$

Here two parameters, p and α' , are needed to describe the turbulence cascade, because the cascade depends on scale for under-developed turbulence. Thus the power spectral index is not linearly related to the second-order structure function exponent (as is the case for fully developed turbulence), but includes spatial inhomogeneity. The intermittency parameter, p , again gives the spatial inhomogeneity of the cascade rate, while the α' parameter is the intrinsic spectral slope describing the scaling properties of the space-averaged cascade rate. The first terms on the right-hand sides of the previous two equations now represent scale dependence of the cascade, and the second terms represent intermittency. The spectral index is related to the intrinsic spectral index and p parameter in the Kolmogorov's form

$$\alpha = \alpha' + \frac{1}{3} - \log_2(p^{2/3} + (1-p)^{2/3}) \quad (6)$$

and in the Kraichnan–Iroshnikov form

$$\alpha = \alpha' + \frac{1}{2} - \log_2(p^{2/3} + (1-p)^{1/2}) \quad (7)$$

Structure functions up to $m = 4$ only have been calculated since our 1-hour data intervals (with sampling resolution of 0.092 s) include only approximately 39,130 data points (see e.g. discussion in Horbury and Balogh, 1997). **The scaling indices are calculated over timescales from 6 to 96 s, within the inertial range (see Section 3.3). The results are given for the total structure function obtained by summing together structure functions of the three components of the magnetic field as e.g., in Pei et al. (2016).**

In Figure 6, the standard p -model scaling exponent curves are plotted as a function of m for $p = 0.5-1$. The observational results are shown as lime-green crosses (solar wind ahead) and dots (sheath subregions). Orange curves correspond to Kolmogorov (K) scalings and blue curves correspond to Kraichnan–Iroshnikov (K–I) scalings for varying amounts of intermittency, p . The grey horizontal line gives the maximum-intermittency case (i.e., $p = 1; g(m) = 1$), and the pink and cyan curves the non-intermittent (i.e., $p = 0.5$) cases corresponding to Kolmogorov and Kraichnan–Iroshnikov turbulence, respectively. The thick black curves show the best non-linear least squares fits to the extended p -model.

We note that, for the majority of cases, the standard p -model curves do not match well with the observed $g(m)$ -curve (lime dots and crosses); there is either significant deviations between the observed and modelled points, or the observed points do not follow the model trends, or both. **The best agreement with the standard p -model is with the solar wind ahead of the fast sheath, being consistent with the Kolmogorov form at high p -values (~ 0.85). The Near-Shock region of the fast sheath and the solar wind ahead the slow sheath coincide in turn relatively closely with the Kraichnan form of the standard p -model, also at high p -values. In all other cases the observed values deviate from the standard p -model curves in particular deeper in the fast sheath.**

In both intermittent and non-intermittent cases, the structure function should have either $g(3) = 1$ for the Kolmogorov scaling or $g(4) = 1$ for the Kraichnan–Iroshnikov scaling. There are several regions in our data events for which neither $g(3) \approx 1$ nor $g(4) \approx 1$ hold. **We note that significant deviations from these values can give rise to false non-intermittent signatures, as discussed e.g. in Pagel and Balogh (2002).**

The extended p -model can be fitted with the data with excellent agreement and the Kolmogorov and Kraichnan–Iroshnikov forms overlap (black thick curve). However, these two forms of the model yield very different p and α values; these values

are given in the panels of Figure 6, with the corresponding standard deviation errors in parenthesis. The errors are of the order 10^{-3} . We note that the Kraichnan–Iroshnikov form fits yield consistently larger p -values than the Kolmogorov form fits, but both indicate high intermittency. The values of spectral indices given by the Kraichnan–Iroshnikov form are however clearly more consistent with the spectral indices shown in Table 2 that were calculate for the fitting for $\langle \delta B \rangle$ using the same
5 timescale range.

4 Discussion

We have investigated magnetic field fluctuations in three CME-driven sheath regions observed in the solar wind at the Lagrange L1 point. Three parts of the sheath were studied separately, corresponding to the regions just adjacent to the shock (Near-Shock), at or near the middle of the sheath (Mid-Sheath), and adjacent to the ejecta leading edge (Near-LE). The results were
10 also compared with the solar wind preceding the sheaths.

For all three cases, we found that the spectral and turbulent properties were considerably different between the preceding solar wind and the sheath. This was the case despite very different overall event properties, e.g., speed of the sheath and preceding shock, shock angle and strength, level of upstream fluctuations and upstream solar wind speed and plasma beta. This is in contrast with the sheath analysed by Good et al. (2020), who found clear differences between the solar wind ahead
15 and in the sheath at the orbit of Mercury, but not near the orbit of Earth. However, they investigated fluctuations throughout the sheath collectively, while we have investigated three subregions separately. The sheath analysed in their work was slow and, at Earth’s orbit, the preceding shock had a quasi-perpendicular configuration. We emphasised that in our study some clear changes between the solar wind ahead and the Near-Shock subregion in particular occurred also for the slowest sheath that was preceded by an almost-perpendicular shock.

20 Firstly, distributions of normalised magnetic field fluctuations were flatter and spread to considerably higher values in the Near-Shock region than in the preceding solar wind for all events. For the fast sheath in particular $\delta B/B > 2$ values demonstrated the existence of significant rotations and compressional fluctuations. This is expected as the processes at the shock are more efficient the faster and stronger the shock is, e.g., fast shocks are expected to cause more efficiently alignment and amplification of pre-existing solar wind discontinuities, provide more free-energy for wave generation, etc. (e.g., Neugebauer
25 et al., 1993; Kataoka et al., 2005; Kilpua et al., 2013; Ala-Lahti et al., 2018, 2019). The quasi-parallel nature of the shock could have also enhanced the fluctuations for the fast event. For all cases, the distribution of the magnetic field fluctuations in the Near-LE region appear quite similar to those in the pre-existing solar wind (consistent with the PVI results). The kurtosis analysis revealed further details as more peaked Near-LE distributions for medium and slow sheaths. We also note that in the inertial range spectral indices were the most similar between the solar wind ahead and the Near-LE region. This could be
30 understood considering that the part of the sheath closest to the ejecta leading edge is not affected by the shock and for the slower sheaths processes at the leading edge do not affect that much either. The Near-LE region of the fast sheath had however distinctly flat $\delta B/B$ distributions and extended tails when compared to the solar wind ahead and the slower sheaths. This could indicate effective magnetic field draping process about the CME ejecta. As discussed by Gosling and McComas (1987) and

McComas et al. (1988), the amount of draping increases with the CME speed. The detailed connection of the draping to sheath small-scale structures has however not yet been established. The mean amplitudes and normalised amplitudes of fluctuations were higher in the sheath than in the preceding solar wind, which is expected as the shock compresses the plasma and field ahead.

5 The compressibility $\langle \delta|B|/\delta B \rangle$ was also generally higher in the sheath than in the preceding solar wind, suggesting that the new fluctuations that were generated in the transition from the solar wind ahead to the ejecta were mostly compressible. We also found that, in terms of compressibility, sheaths behave more like the slow solar wind than the fast wind, i.e., we found $\langle \delta|B|/\delta B \rangle$ values above 0.2 to dominate in the sheath, in agreement with what is found for the slow wind (Bavassano et al., 1982; Bruno and Carbone, 2013). This was the case also for the fastest sheath in our study that was preceded by fast wind, with
10 $\langle \delta|B|/\delta B \rangle$ values below 0.2.

The inertial range spectral indices in our study for sheath subregions were mostly clearly steeper than Kolmogorov's spectral index of -1.67 . Borovsky (2012) reported steeper slopes for the magnetic field fluctuations for the slow solar wind (spectral index -1.7) than for the fast wind (spectral index -1.54). This also suggests that turbulence in sheaths resembles more turbulence in the slow wind than in the fast wind. We however emphasise that spectral indices in our study exhibited quite large
15 variability. Interestingly also, the fast solar wind ahead the fast sheath had steeper spectral index than the slow solar wind ahead the medium-speed and slow sheaths, which had their spectral indices close to Kraichnan–Iroshnikov's and Kolmogorov's values, respectively. This could be however related to interference of foreshock waves. The kinetic range spectral indices in turn indicated consistently shallower slopes (spectral indices varying from about -2.1 to -2.5) than what is on average observed in the solar wind (spectral index ~ -2.8 , see Section 3.3). Several previous studies have also reported that in the solar wind
20 both kinetic and inertial spectral indices exhibit large range of values (e.g., Leamon et al., 1998; Smith et al., 2006; Borovsky, 2012). This is the case also in the magnetosheath (e.g., Alexandrova et al., 2008). The inertial range spectral indices in the solar wind tend to also steepen towards Kolmogorov's with increasing distance from the Sun (e.g., Bavassano et al., 1982). Sahraoui et al. (2009) reported average spectral indices matching our values (from -2.3 to -2.5) in their study of magnetic field fluctuations in the near-Earth solar wind using Cluster observations for about a 3-h time interval in the frequency range
25 4–35 Hz (i.e. 2.5–0.03 s). They observed another spectral breakpoint at 35 Hz, close to the electron gyro-scale, after which the slopes further steepened with the spectral index ~ -3.8 (see also Sahraoui et al., 2010; Alexandrova et al., 2013; Bruno et al., 2017). Sahraoui et al. (2009) argued that only a relatively small part of the energy is damped at ion scales where kinetic Alfvén wave cascade still occurs from larger to smaller scales, whereas most of the dissipation occurs in the electron scales where the observed slopes were much steeper. The observations we used in our study are not high-cadence enough to capture this second
30 breakpoint, but the kinetic range spectral indices being close to Sahraoui et al. (2009) implies that this could be generally the case also for CME-driven sheath regions. The statistical study of Huang et al. (2017) found that in the Earth's magnetosheath in the inertial scale the spectral indices were close to -1 , resembling thus the energy driven scale in the solar wind rather than Kolmogorov's $-5/3$. Spectral indices close to Kolmogorov's were observed only further away from the bow shock at the flanks and close to the magnetopause. The majority of the events were dominated by compressible magnetosonic-like fluctuations.

We investigated intermittency using various methods. Firstly, we found that the PVI values are generally high in the sheaths when compared to the ambient solar wind, suggesting that sheaths embed frequently intermittent structures. This is in agreement with Zhou et al. (2019). Our analysis of kurtosis and distributions of normalised fluctuations also suggests that sheaths have in general high intermittency. Generally, intermittency decreases with distance from the Sun and is higher in the fast than in the slow wind, suggesting that it has largely origin at the Sun (Pagel and Balogh, 2001; Wawrzaszek et al., 2015; Bruno, 2019). The slow wind in turn shows strong variability in its intermittency (e.g., Pagel and Balogh, 2002). The fact that CME-driven sheaths feature high intermittency at 1 AU suggests that intermittent structures are actively formed during the formation and evolution of sheaths in interplanetary space. This is consistent with sheaths being heliospheric structures that gather over long periods of time (up to several days near Earth’s orbit) from inhomogeneous solar wind plasma that gets compressed and processed at the CME shock and then piles up at the ejecta leading edge. Good et al. (2020) also found an increase in intermittency for their slow CME sheath from Mercury’s to Earth’s orbit. The authors suggested that it likely is due to the development of intermittent structures, e.g. current sheets in the sheath during CME propagation. **This scenario is consistent with generally steep inertial range spectral indices in CME-driven sheaths as current. As suggested by e.g., the analysis in Li et al. (2012) current sheets in the solar wind could generally steepen the spectra. We also note that our analysis hinted that intermittency in B_z is larger than in B_x or B_y . This is an interesting point for future research and could be related to processes in action at the shock and/or CME leading edge creating in particular out-of-ecliptic magnetic field fluctuations (e.g., field line draping discussed in the Introduction).**

Our structure function analysis showed that the standard p -model did not generally match the observed $g(m)$ curve features. The best match was found for the fast solar wind preceding the fast sheath. The extended p -model however yielded a very good fit both for the Kolmogorov and Kraichnan–Iroshnikov forms, and the curves were indistinguishable. This has been the case also in some previous studies in the solar wind (e.g., Horbury and Balogh, 1997; Horbury et al., 1997), and reported also for the studies of turbulence in Earth’s magnetosheath (e.g., Yordanova et al., 2008) and in the magnetospheric cusp (e.g., Yordanova et al., 2004). In addition, Kraichnan–Iroshnikov form yielded consistently larger intermittency parameter p and α values, also reported earlier (e.g., Tu et al., 1996; Yordanova et al., 2004). They also matched clearly better with the indices we obtained from the fitting of the mean magnetic field fluctuations for the corresponding timescales. **These findings would suggest that turbulence in the sheath is not fully developed at the orbit of Earth and is more consistent with the Kraichnan–Iroshnikov picture than Kolmogorov’s, i.e. sheaths would behave more like a magnetofluid, which would agree with sheaths being high magnetic field structures.** We note that previous studies have also reported that the Kraichnan–Iroshnikov form produces better fits in particular in cases of solar wind periods with strong magnetic field (e.g., Podesta, 2011). **The results are however partly contradictory in the sense that the slopes were Kraichnan–Iroshnikov like (-1.5) only for a few cases. It could be that CME driven sheaths can embed plenty of structures (current sheets with large amplitude and large angle directional field changes, magnetic holes, reconnection exhausts, plasma interfaces, plasma blobs) even in relatively short periods of time and are thus not described so well by the current turbulent models. Li et al. (2012) also suggested that Kolmogorov-like spectra in the solar wind could also result from the presence of intermittent current**

sheets were the field direction changes rapidly. I.e., as a consequence, the spectra would steepen from Kraichnan to Kolmogorov.

Our study highlights that turbulent properties can vary strongly within the sheath and are controlled by various factors, including the properties of the solar wind ahead, e.g. its plasma beta and level of turbulence, the shock strength and configuration, path of the spacecraft through the shock–sheath–ejecta structure, and the properties of the driving CME ejecta, in particular by its speed (Kilpua et al., 2013; Moissard et al., 2019). The variations were in general most drastic for the fastest sheath and most subtle for the slowest sheath in our study. We emphasise that we investigated here only one subregion in the middle of the sheath and it would be interesting to study how turbulent properties vary across the whole sheath from the shock to the ejecta leading edge, e.g. by applying a sliding window. Our study also revealed a small-scale coherent structure within the December 14, 2006 fast sheath. This substructure had distinct properties featuring e.g., clearly depressed $\delta B/B$ values, high compressibility and very shallow spectral slope with inertial range spectral index close to Kraichnan–Iroshnikov’s $-3/2$ value. Regarding intermittency, compressibility and general absence of Kolmogorov’s type turbulence CME sheaths (in particular in regions close to the shock) are similar to planetary magnetosheath, which implies universality of those properties in a compressible medium, and also the universality regarding the role of the shock on destroying the correlation between the turbulent fluctuations in the solar wind as discussed in Huang et al. (2017). The f^{-1} spectrum was however not found.

5 Summary

To summarise, based on our case study of three CME-driven sheath regions observed at the Lagrange L1 point, the magnetic field fluctuation amplitudes, normalised fluctuation amplitudes, and compressibility are enhanced in the sheath when compared to the solar wind ahead. The transition to the sheath thus generates new fluctuations and/or amplifies (in magnitude and/or change in the field direction) of pre-existing fluctuations relative to the mean field. The intermittency was also found to be higher in the sheath than in the preceding solar wind for many of the investigated subregions. These findings applied for all three sheaths involved, featuring different speeds, shock strengths, and shock angles. Turbulent properties and spectral indices varied also quite considerably between the studied events and the sheath subregions, which reflects the complex structure and formation process of the sheaths of various properties. In general, turbulence in sheaths resembles rather that of the slow solar wind, and we found this to be valid even for the fast sheath preceded by fast wind. According to our study, turbulence in the sheath is not fully developed, likely due to processes that are constantly in action at the shock and close to the ejecta leading edge as the CME ploughs its way through interplanetary space. This can also explain the high intermittency in sheaths. We also found indications that in sheaths the energy cascade from larger to smaller scales could still be partly on-going at the ion scales, which suggests that the majority of the dissipation would occur at electron scales (not captured by our study).

Future studies focusing deeper on how sheath turbulence varies from the shock to the ejecta leading and extensive statistical studies connecting sheath properties to preceding solar wind and driver characteristics would shed light on these issues. Parker Solar Probe (Fox et al., 2016) and Solar Orbiter (Müller et al., 2013) will also make it possible to analyse sheath properties and

turbulence with varying heliospheric distances and possibly provide multi-spacecraft encounters of CME sheaths, allowing to probe how sheath characteristics evolve from the nose of the shock to the CME flanks.

Competing interests. The authors declare that they have no conflict of interest.

Acknowledgements. The results presented in here have been achieved under the framework of the Finnish Centre of Excellence in Research of Sustainable Space (Academy of Finland grant number 1312390), which we gratefully acknowledge. This project has received funding from the European Research Council (ERC) under the European Union's Horizon 2020 research and innovation programme (ERC-COG 724391). E. K. J. Kilpua acknowledges Academy of Finland project SMASH no. 310445. E. Palmerio's research was supported by the NASA Living With a Star Jack Eddy Postdoctoral Fellowship Program, administered by UCAR's Cooperative Programs for the Advancement of Earth System Science (CPAESS) under award no. NNX16AK22G. E. Yordanova's research was supported by the Swedish Civil Contingencies Agency (MSB, Dnr.2016-2102).

References

- Ala-Lahti, M., Kilpua, E. K. J., Souček, J., Pulkkinen, T. I., and Dimmock, A. P.: Alfvén Ion Cyclotron Waves in Sheath Regions Driven by Interplanetary Coronal Mass Ejections, *J. Geophys. Res.-Space*, 124, 3893–3909, <https://doi.org/10.1029/2019JA026579>, 2019.
- Ala-Lahti, M. M., Kilpua, E. K. J., Dimmock, A. P., Osmane, A., Pulkkinen, T., and Souček, J.: Statistical analysis of mirror mode waves in sheath regions driven by interplanetary coronal mass ejection, *Ann. Geophys.*, 36, 793–808, <https://doi.org/10.5194/angeo-36-793-2018>, 2018.
- Alexandrova, O., Lacombe, C., and Mangeney, A.: Spectra and anisotropy of magnetic fluctuations in the Earth’s magnetosheath: Cluster observations, *Ann. Geophys.*, 26, 3585–3596, <https://doi.org/10.5194/angeo-26-3585-2008>, 2008.
- Alexandrova, O., Chen, C. H. K., Sorriso-Valvo, L., Horbury, T. S., and Bale, S. D.: Solar Wind Turbulence and the Role of Ion Instabilities, *Space Sci. Rev.*, 178, 101–139, <https://doi.org/10.1007/s11214-013-0004-8>, 2013.
- Alves, L. R., Da Silva, L. A., Souza, V. M., Sibeck, D. G., Jauer, P. R., Vieira, L. E. A., Walsh, B. M., Silveira, M. V. D., Marchezi, J. P., Rockenbach, M., Lago, A. D., Mendes, O., Tsurutani, B. T., Koga, D., Kanekal, S. G., Baker, D. N., Wygant, J. R., and Kletzing, C. A.: Outer radiation belt dropout dynamics following the arrival of two interplanetary coronal mass ejections, *Geophys. Res. Lett.*, 43, 978–987, <https://doi.org/10.1002/2015GL067066>, 2016.
- Bale, S. D., Balikhin, M. A., Horbury, T. S., Krasnoselskikh, V. V., Kucharek, H., Möbius, E., Walker, S. N., Balogh, A., Burgess, D., Lembège, B., Lucek, E. A., Scholer, M., Schwartz, S. J., and Thomsen, M. F.: Quasi-perpendicular Shock Structure and Processes, *Space Sci. Rev.*, 118, 161–203, <https://doi.org/10.1007/s11214-005-3827-0>, 2005a.
- Bale, S. D., Kellogg, P. J., Mozer, F. S., Horbury, T. S., and Reme, H.: Measurement of the Electric Fluctuation Spectrum of Magnetohydrodynamic Turbulence, *Phys. Rev. Lett.*, 94, 215002, <https://doi.org/10.1103/PhysRevLett.94.215002>, 2005b.
- Bavassano, B., Dobrowolny, M., Mariani, F., and Ness, N. F.: Radial evolution of power spectra of interplanetary Alfvénic turbulence, *J. Geophys. Res.-Space*, 87, 3617–3622, <https://doi.org/10.1029/JA087iA05p03617>, 1982.
- Borovsky, J. E.: The velocity and magnetic field fluctuations of the solar wind at 1 AU: Statistical analysis of Fourier spectra and correlations with plasma properties, *J. Geophys. Res.-Space*, 117, A05104, <https://doi.org/10.1029/2011JA017499>, 2012.
- Bruno, R.: Intermittency in Solar Wind Turbulence From Fluid to Kinetic Scales, *Earth Space Sci.*, 6, 656–672, <https://doi.org/10.1029/2018EA000535>, 2019.
- Bruno, R. and Carbone, V.: The Solar Wind as a Turbulence Laboratory, *Living Rev. Sol. Phys.*, 10, 2, <https://doi.org/10.12942/lrsp-2013-2>, 2013.
- Bruno, R., Telloni, D., DeIure, D., and Pietropaolo, E.: Solar wind magnetic field background spectrum from fluid to kinetic scales, *Mon. Not. Roy. Astron. Soc.*, 472, 1052–1059, <https://doi.org/10.1093/mnras/stx2008>, 2017.
- Bruno, R., Telloni, D., Sorriso-Valvo, L., Marino, R., De Marco, R., and D’Amicis, R.: The low-frequency break observed in the slow solar wind magnetic spectra, *Astron. Astrophys.*, 627, A96, <https://doi.org/10.1051/0004-6361/201935841>, 2019.
- Burgess, D., Lucek, E. A., Scholer, M., Bale, S. D., Balikhin, M. A., Balogh, A., Horbury, T. S., Krasnoselskikh, V. V., Kucharek, H., Lembège, B., Möbius, E., Schwartz, S. J., Thomsen, M. F., and Walker, S. N.: Quasi-parallel Shock Structure and Processes, *Space Sci. Rev.*, 118, 205–222, <https://doi.org/10.1007/s11214-005-3832-3>, 2005.
- Burlaga, L. F.: Intermittent turbulence in the solar wind, *J. Geophys. Res.-Space*, 96, 5847–5851, <https://doi.org/10.1029/91JA00087>, 1991.
- Carbone, V.: Cascade model for intermittency in fully developed magnetohydrodynamic turbulence, *Phys. Rev. Lett.*, 71, 1546–1548, <https://doi.org/10.1103/PhysRevLett.71.1546>, 1993.

- Chen, C. H. K., Matteini, L., Burgess, D., and Horbury, T. S.: Magnetic field rotations in the solar wind at kinetic scales, *Mon. Not. Roy. Astron. Soc.*, 453, L64–L68, <https://doi.org/10.1093/mnrasl/slv107>, 2015.
- Coleman, Paul J., J.: Turbulence, Viscosity, and Dissipation in the Solar-Wind Plasma, *Astrophys. J.*, 153, 371, <https://doi.org/10.1086/149674>, 1968.
- 5 Echer, E., Gonzalez, W. D., and Tsurutani, B. T.: Interplanetary conditions leading to superintense geomagnetic storms ($Dst < -250$ nT) during solar cycle 23, *Geophys. Res. Lett.*, 35, L06S03, <https://doi.org/10.1029/2007GL031755>, 2008.
- Feng, H. and Wang, J.: Magnetic-reconnection exhausts in the sheath of magnetic clouds, *Astron. Astrophys.*, 559, A92, <https://doi.org/10.1051/0004-6361/201322522>, 2013.
- Feynman, J. and Ruzmaikin, A.: Distribution of the interplanetary magnetic field revisited, *J. Geophys. Res.-Space*, 99, 17 645–17 652, <https://doi.org/10.1029/94JA01098>, 1994.
- 10 Fox, N. J., Velli, M. C., Bale, S. D., Decker, R., Driesman, A., Howard, R. A., Kasper, J. C., Kinnison, J., Kusterer, M., Lario, D., Lockwood, M. K., McComas, D. J., Raouafi, N. E., and Szabo, A.: The Solar Probe Plus Mission: Humanity’s First Visit to Our Star, *Space Sci. Rev.*, 204, 7–48, <https://doi.org/10.1007/s11214-015-0211-6>, 2016.
- Frisch, U., Sulem, P. L., and Nelkin, M.: A simple dynamical model of intermittent fully developed turbulence, *J. Fluid Mech.*, 87, 719–736, <https://doi.org/10.1017/S0022112078001846>, 1978.
- 15 Good, S. W., Ala-Lahti, M., Palmerio, E., Kilpua, E. K. J., and Osmane, A.: Radial Evolution of Magnetic Field Fluctuations in an Interplanetary Coronal Mass Ejection Sheath, *Astrophys. J.*, 893, 110, <https://doi.org/10.3847/1538-4357/ab7fa2>, 2020.
- Gosling, J. T. and McComas, D. J.: Field line draping about fast coronal mass ejecta - A source of strong out-of-the-ecliptic interplanetary magnetic fields, *Geophys. Res. Lett.*, 14, 355–358, <https://doi.org/10.1029/GL014i004p00355>, 1987.
- 20 Greco, A., Chuychai, P., Matthaeus, W. H., Servidio, S., and Dmitruk, P.: Intermittent MHD structures and classical discontinuities, *Geophys. Res. Lett.*, 35, L19111, <https://doi.org/10.1029/2008GL035454>, 2008.
- Greco, A., Matthaeus, W. H., Perri, S., Osman, K. T., Servidio, S., Wan, M., and Dmitruk, P.: Partial Variance of Increments Method in Solar Wind Observations and Plasma Simulations, *Space Sci. Rev.*, 214, 1, <https://doi.org/10.1007/s11214-017-0435-8>, 2018.
- Hietala, H., Kilpua, E. K. J., Turner, D. L., and Angelopoulos, V.: Depleting effects of ICME-driven sheath regions on the outer electron 25 radiation belt, *Geophys. Res. Lett.*, 41, 2258–2265, <https://doi.org/10.1002/2014GL059551>, 2014.
- Horbury, T. S. and Balogh, A.: Structure function measurements of the intermittent MHD turbulent cascade, *Nonlin. Processes Geophys.*, 4, 185–199, <https://doi.org/10.5194/npg-4-185-1997>, 1997.
- Horbury, T. S. and Balogh, A.: Evolution of magnetic field fluctuations in high-speed solar wind streams: Ulysses and Helios observations, *J. Geophys. Res.-Space*, 106, 15 929–15 940, <https://doi.org/10.1029/2000JA000108>, 2001.
- 30 Horbury, T. S., Balogh, A., Forsyth, R. J., and Smith, E. J.: ULYSSES observations of intermittent heliospheric turbulence, *Adv. Space Res.*, 19, 847–850, [https://doi.org/10.1016/S0273-1177\(97\)00290-1](https://doi.org/10.1016/S0273-1177(97)00290-1), 1997.
- Horbury, T. S., Forman, M. A., and Oughton, S.: Spacecraft observations of solar wind turbulence: an overview, *Plasma Phys. Control. Fusion*, 47, B703–B717, <https://doi.org/10.1088/0741-3335/47/12B/S52>, 2005.
- Howes, G. G., Klein, K. G., and TenBarge, J. M.: Validity of the Taylor Hypothesis for Linear Kinetic Waves in the Weakly Collisional Solar 35 Wind, *Astrophys. J.*, 789, 106, <https://doi.org/10.1088/0004-637X/789/2/106>, 2014.
- Huang, S. Y., Hadid, L. Z., Sahraoui, F., Yuan, Z. G., and Deng, X. H.: On the Existence of the Kolmogorov Inertial Range in the Terrestrial Magnetosheath Turbulence, *Astrophys. J. Lett.*, 836, L10, <https://doi.org/10.3847/2041-8213/836/1/L10>, 2017.

- Huttunen, K. and Koskinen, H.: Importance of post-shock streams and sheath region as drivers of intense magnetospheric storms and high-latitude activity, *Ann. Geophys.*, 22, 1729–1738, <https://doi.org/10.5194/angeo-22-1729-2004>, 2004.
- Huttunen, K. E. J., Koskinen, H. E. J., and Schwenn, R.: Variability of magnetospheric storms driven by different solar wind perturbations, *J. Geophys. Res.-Space*, 107, 1121, <https://doi.org/10.1029/2001JA900171>, 2002.
- 5 Iroshnikov, P. S.: Turbulence of a Conducting Fluid in a Strong Magnetic Field, *Soviet Astron.*, 7, 566, 1964.
- Jones, G. H. and Balogh, A.: Context and heliographic dependence of heliospheric planar magnetic structures, *J. Geophys. Res.-Space*, 105, 12 713–12 724, <https://doi.org/10.1029/2000JA900003>, 2000.
- Kalliokoski, M. M. H., Kilpua, E. K. J., Osmane, A., Turner, D. L., Jaynes, A. N., Turc, L., George, H., and Palmroth, M.: Outer radiation belt and inner magnetospheric response to sheath regions of coronal mass ejections: a statistical analysis, *Ann. Geophys.*, 38, 683–701, <https://doi.org/10.5194/angeo-38-683-2020>, 2020.
- 10 Kataoka, R., Watari, S., Shimada, N., Shimazu, H., and Marubashi, K.: Downstream structures of interplanetary fast shocks associated with coronal mass ejections, *Geophys. Res. Lett.*, 32, L12103, <https://doi.org/10.1029/2005GL022777>, 2005.
- Kilpua, E., Koskinen, H. E. J., and Pulkkinen, T. I.: Coronal mass ejections and their sheath regions in interplanetary space, *Living Rev. Sol. Phys.*, 14, 5, <https://doi.org/10.1007/s41116-017-0009-6>, 2017a.
- 15 Kilpua, E. K. J., Hietala, H., Koskinen, H. E. J., Fontaine, D., and Turc, L.: Magnetic field and dynamic pressure ULF fluctuations in coronal-mass-ejection-driven sheath regions, *Ann. Geophys.*, 31, 1559–1567, <https://doi.org/10.5194/angeo-31-1559-2013>, 2013.
- Kilpua, E. K. J., Hietala, H., Turner, D. L., Koskinen, H. E. J., Pulkkinen, T. I., Rodriguez, J. V., Reeves, G. D., Claudepierre, S. G., and Spence, H. E.: Unraveling the drivers of the storm time radiation belt response, *Geophys. Res. Lett.*, 42, 3076–3084, <https://doi.org/10.1002/2015GL063542>, 2015.
- 20 Kilpua, E. K. J., Balogh, A., von Steiger, R., and Liu, Y. D.: Geoeffective Properties of Solar Transients and Stream Interaction Regions, *Space Sci. Rev.*, 212, 1271–1314, <https://doi.org/10.1007/s11214-017-0411-3>, 2017b.
- Kilpua, E. K. J., Fontaine, D., Moissard, C., Ala-Lahti, M., Palmerio, E., Yordanova, E., Good, S. W., Kalliokoski, M. M. H., Lumme, E., Osmane, A., Palmroth, M., and Turc, L.: Solar Wind Properties and Geospace Impact of Coronal Mass Ejection-Driven Sheath Regions: Variation and Driver Dependence, *Space Weather*, 17, 1257–1280, <https://doi.org/10.1029/2019SW002217>, 2019a.
- 25 Kilpua, E. K. J., Turner, D. L., Jaynes, A. N., Hietala, H., Koskinen, H. E. J., Osmane, A., Palmroth, M., Pulkkinen, T. I., Vainio, R., Baker, D., and Claudepierre, S. G.: Outer Van Allen Radiation Belt Response to Interacting Interplanetary Coronal Mass Ejections, *J. Geophys. Res.-Space*, 124, 1927–1947, <https://doi.org/10.1029/2018JA026238>, 2019b.
- Kolmogorov, A.: The Local Structure of Turbulence in Incompressible Viscous Fluid for Very Large Reynolds' Numbers, *Akademiia Nauk SSSR Doklady*, 30, 301–305, 1941.
- 30 Kraichnan, R. H.: Inertial-Range Spectrum of Hydromagnetic Turbulence, *Phys. Fluids*, 8, 1385–1387, <https://doi.org/10.1063/1.1761412>, 1965.
- Krommes, J. A.: Fundamental statistical descriptions of plasma turbulence in magnetic fields, *Phys. Rep.*, 360, 1–352, [https://doi.org/10.1016/S0370-1573\(01\)00066-7](https://doi.org/10.1016/S0370-1573(01)00066-7), 2002.
- Leamon, R. J., Smith, C. W., Ness, N. F., Matthaeus, W. H., and Wong, H. K.: Observational constraints on the dynamics of the interplanetary magnetic field dissipation range, *J. Geophys. Res.-Space*, 103, 4775–4788, <https://doi.org/10.1029/97JA03394>, 1998.
- 35 Lepping, R. P., Acuña, M. H., Burlaga, L. F., Farrell, W. M., Slavin, J. A., Schatten, K. H., Mariani, F., Ness, N. F., Neubauer, F. M., Whang, Y. C., Byrnes, J. B., Kennon, R. S., Panetta, P. V., Scheifele, J., and Worley, E. M.: The Wind Magnetic Field Investigation, *Space Sci. Rev.*, 71, 207–229, <https://doi.org/10.1007/BF00751330>, 1995.

- Li, G., Qin, G., Hu, Q., and Miao, B.: Effect of current sheets on the power spectrum of the solar wind magnetic field using a cell model, *Advances in Space Research*, 49, 1327–1332, <https://doi.org/10.1016/j.asr.2012.02.008>, 2012.
- Lugaz, N., Farrugia, C. J., Huang, C.-L., and Spence, H. E.: Extreme geomagnetic disturbances due to shocks within CMEs, *Geophys. Res. Lett.*, 42, 4694–4701, <https://doi.org/10.1002/2015GL064530>, 2015.
- 5 Marsch, E. and Tu, C. Y.: Non-Gaussian probability distributions of solar wind fluctuations, *Ann. Geophys.*, 12, 1127–1138, <https://doi.org/10.1007/s00585-994-1127-8>, 1994.
- Marsch, E. and Tu, C. Y.: Intermittency, non-Gaussian statistics and fractal scaling of MHD fluctuations in the solar wind, *Nonlin. Processes Geophys.*, 4, 101–124, 1997.
- Matteini, L., Stansby, D., Horbury, T. S., and Chen, C. H. K.: On the 1/f Spectrum in the Solar Wind and Its Connection with Magnetic Compressibility, *Astrophys. J. Lett.*, 869, L32, <https://doi.org/10.3847/2041-8213/aaf573>, 2018.
- 10 Matthaeus, W. H. and Goldstein, M. L.: Measurement of the rugged invariants of magnetohydrodynamic turbulence in the solar wind, *J. Geophys. Res.-Space*, 87, 6011–6028, <https://doi.org/10.1029/JA087iA08p06011>, 1982.
- McComas, D. J., Gosling, J. T., Winterhalter, D., and Smith, E. J.: Interplanetary magnetic field draping about fast coronal mass ejecta in the outer heliosphere, *J. Geophys. Res.-Space*, 93, 2519–2526, <https://doi.org/10.1029/JA093iA04p02519>, 1988.
- 15 Meneveau, C. and Sreenivasan, K. R.: Simple multifractal cascade model for fully developed turbulence, *Phys. Rev. Lett.*, 59, 1424–1427, <https://doi.org/10.1103/PhysRevLett.59.1424>, 1987.
- Moissard, C., Fontaine, D., and Savoini, P.: A Study of Fluctuations in Magnetic Cloud-Driven Sheaths, *J. Geophys. Res.-Space*, 124, 8208–8226, <https://doi.org/10.1029/2019JA026952>, 2019.
- Müller, D., Marsden, R. G., St. Cyr, O. C., and Gilbert, H. R.: Solar Orbiter . Exploring the Sun-Heliosphere Connection, *Sol. Phys.*, 285, 25–70, <https://doi.org/10.1007/s11207-012-0085-7>, 2013.
- 20 Nakagawa, T., Nishida, A., and Saito, T.: Planar magnetic structures in the solar wind, *J. Geophys. Res.-Space*, 94, 11 761–11 775, <https://doi.org/10.1029/JA094iA09p11761>, 1989.
- Neugebauer, M., Clay, D. R., and Gosling, J. T.: The origins of planar magnetic structures in the solar wind, *J. Geophys. Res.-Space*, 98, 9383–9390, <https://doi.org/10.1029/93JA00216>, 1993.
- 25 Nikolaeva, N. S., Yermolaev, Y. I., and Lodkina, I. G.: Dependence of geomagnetic activity during magnetic storms on the solar wind parameters for different types of streams, *Geomagnetism Aeronomy*, 51, 49–65, <https://doi.org/10.1134/S0016793211010099>, 2011.
- Ogilvie, K. W. and Desch, M. D.: The wind spacecraft and its early scientific results, *Adv. Space Res.*, 20, 559–568, [https://doi.org/10.1016/S0273-1177\(97\)00439-0](https://doi.org/10.1016/S0273-1177(97)00439-0), 1997.
- Ogilvie, K. W., Chornay, D. J., Fritzenreiter, R. J., Hunsaker, F., Keller, J., Lobell, J., Miller, G., Scudder, J. D., Sittler, E. C., J., Torbert, R. B., Bodet, D., Needell, G., Lazarus, A. J., Steinberg, J. T., Tappan, J. H., Mavretic, A., and Gergin, E.: SWE, A Comprehensive Plasma Instrument for the Wind Spacecraft, *Space Sci. Rev.*, 71, 55–77, <https://doi.org/10.1007/BF00751326>, 1995.
- 30 Osmane, A., Dimmock, A. P., and Pulkkinen, T. I.: Universal properties of mirror mode turbulence in the Earth’s magnetosheath, *Geophys. Res. Lett.*, 42, 3085–3092, <https://doi.org/10.1002/2015GL063771>, 2015.
- Pagel, C. and Balogh, A.: A study of magnetic fluctuations and their anomalous scaling in the solar wind: the Ulysses fast-latitude scan, *Nonlin. Processes Geophys.*, 8, 313–330, 2001.
- 35 Pagel, C. and Balogh, A.: Intermittency in the solar wind: A comparison between solar minimum and maximum using Ulysses data, *J. Geophys. Res.-Space*, 107, 1178, <https://doi.org/10.1029/2002JA009331>, 2002.

- Paladin, G. and Vulpiani, A.: Anomalous scaling laws in multifractal objects, *Phys. Rep.*, 156, 147–225, [https://doi.org/10.1016/0370-1573\(87\)90110-4](https://doi.org/10.1016/0370-1573(87)90110-4), 1987.
- Palmerio, E., Kilpua, E. K. J., and Savani, N. P.: Planar magnetic structures in coronal mass ejection-driven sheath regions, *Ann. Geophys.*, 34, 313–322, <https://doi.org/10.5194/angeo-34-313-2016>, 2016.
- 5 Pei, Z., He, J., Wang, X., Tu, C., Marsch, E., Wang, L., and Yan, L.: Influence of intermittency on the anisotropy of magnetic structure functions of solar wind turbulence, *J. Geophys. Res.-Space*, 121, 911–924, <https://doi.org/10.1002/2015JA021057>, 2016.
- Podesta, J. J.: On the energy cascade rate of solar wind turbulence in high cross helicity flows, *J. Geophys. Res.-Space*, 116, A05101, <https://doi.org/10.1029/2010JA016306>, 2011.
- Riazantseva, M. O., Rakhmanova, L. S., Zastenker, G. N., Yermolaev, Y. I., and Lodkina, I. G.: Features of the Spectral Characteristics of Plasma Fluctuations in Different Large-Scale Streams of the Solar Wind, *Geomagnetism Aeronomy*, 59, 127–135, <https://doi.org/10.1134/S0016793219020117>, 2019.
- 10 Richardson, I. G.: Solar wind stream interaction regions throughout the heliosphere, *Living Rev. Sol. Phys.*, 15, 1, <https://doi.org/10.1007/s41116-017-0011-z>, 2018.
- Richardson, I. G. and Cane, H. V.: Near-Earth Interplanetary Coronal Mass Ejections During Solar Cycle 23 (1996–2009): Catalog and Summary of Properties, *Sol. Phys.*, 264, 189–237, <https://doi.org/10.1007/s11207-010-9568-6>, 2010.
- 15 Sahraoui, F., Goldstein, M. L., Robert, P., and Khotyaintsev, Y. V.: Evidence of a Cascade and Dissipation of Solar-Wind Turbulence at the Electron Gyroscale, *Phys. Rev. Lett.*, 102, 231102, <https://doi.org/10.1103/PhysRevLett.102.231102>, 2009.
- Sahraoui, F., Goldstein, M. L., Belmont, G., Canu, P., and Rezeau, L.: Three Dimensional Anisotropic k Spectra of Turbulence at Subproton Scales in the Solar Wind, *Phys. Rev. Lett.*, 105, 131101, <https://doi.org/10.1103/PhysRevLett.105.131101>, 2010.
- 20 She, Z.-S. and Leveque, E.: Universal scaling laws in fully developed turbulence, *Phys. Rev. Lett.*, 72, 336–339, <https://doi.org/10.1103/PhysRevLett.72.336>, 1994.
- Siscoe, G. and Odstrcil, D.: Ways in which ICME sheaths differ from magnetosheaths, *J. Geophys. Res.-Space*, 113, A00B07, <https://doi.org/10.1029/2008JA013142>, 2008.
- Siscoe, G., MacNeice, P. J., and Odstrcil, D.: East-west asymmetry in coronal mass ejection geoeffectiveness, *Space Weather*, 5, S04002, <https://doi.org/10.1029/2006SW000286>, 2007.
- 25 Smith, C. W., Hamilton, K., Vasquez, B. J., and Leamon, R. J.: Dependence of the Dissipation Range Spectrum of Interplanetary Magnetic Fluctuations on the Rate of Energy Cascade, *Astrophys. J. Lett.*, 645, L85–L88, <https://doi.org/10.1086/506151>, 2006.
- Sorriso-Valvo, L., Carbone, V., Giuliani, P., Veltri, P., Bruno, R., Antoni, V., and Martines, E.: Intermittency in plasma turbulence, *Planet. Space Sci.*, 49, 1193–1200, [https://doi.org/10.1016/S0032-0633\(01\)00060-5](https://doi.org/10.1016/S0032-0633(01)00060-5), 2001.
- 30 Sorriso-Valvo, L., Carbone, V., and Bruno, R.: On the Origin of the Strong Intermittent Nature of Interplanetary Magnetic Field, *Space Sci. Rev.*, 121, 49–53, <https://doi.org/10.1007/s11214-006-5559-1>, 2005.
- Taylor, G. I.: Production and Dissipation of Vorticity in a Turbulent Fluid, *Proc. R. Soc. Lond. A*, 164, 15–23, <https://doi.org/10.1098/rspa.1938.0002>, 1938.
- Tsurutani, B. T., Gonzalez, W. D., Tang, F., Akasofu, S. I., and Smith, E. J.: Origin of interplanetary southward magnetic fields responsible for major magnetic storms near solar maximum (1978-1979), *J. Geophys. Res.-Space*, 93, 8519–8531, <https://doi.org/10.1029/JA093iA08p08519>, 1988.
- 35

- Tsurutani, B. T., Lakhina, G. S., Sen, A., Hellinger, P., Glassmeier, K.-H., and Mannucci, A. J.: A Review of Alfvénic Turbulence in High-Speed Solar Wind Streams: Hints From Cometary Plasma Turbulence, *J. Geophys. Res.-Space*, 123, 2458–2492, <https://doi.org/10.1002/2017JA024203>, 2018.
- Tu, C.-Y., Marsch, E., and Rosenbauer, H.: An extended structure-function model and its application to the analysis of solar wind intermittency properties, *Ann. Geophys.*, 14, 270–285, <https://doi.org/10.1007/s00585-996-0270-9>, 1996.
- Turner, D. L., Kilpua, E. K. J., Hietala, H., Claudepierre, S. G., O’Brien, T. P., Fennell, J. F., Blake, J. B., Jaynes, A. N., Kanekal, S., Baker, D. N., Spence, H. E., Ripoll, J.-F., and Reeves, G. D.: The Response of Earth’s Electron Radiation Belts to Geomagnetic Storms: Statistics From the Van Allen Probes Era Including Effects From Different Storm Drivers, *J. Geophys. Res.-Space*, 124, 1013–1034, <https://doi.org/10.1029/2018JA026066>, 2019.
- 10 Verscharen, D., Klein, K. G., and Maruca, B. A.: The multi-scale nature of the solar wind, *Living Rev. Sol. Phys.*, 16, 5, <https://doi.org/10.1007/s41116-019-0021-0>, 2019.
- Wawrzaszek, A., Echim, M., Macek, W. M., and Bruno, R.: Evolution of Intermittency in the Slow and Fast Solar Wind beyond the Ecliptic Plane, *Astrophys. J. Lett.*, 814, L19, <https://doi.org/10.1088/2041-8205/814/2/L19>, 2015.
- Yermolaev, Y. I., Nikolaeva, N. S., Lodkina, I. G., and Yermolaev, M. Y.: Specific interplanetary conditions for CIR-, Sheath-, and ICME-induced geomagnetic storms obtained by double superposed epoch analysis, *Ann. Geophys.*, 28, 2177–2186, <https://doi.org/10.5194/angeo-28-2177-2010>, 2010.
- 15 Yordanova, E., Grzesiak, M., Wernik, A., Popielawska, B., and Stasiewicz, K.: Multifractal structure of turbulence in the magnetospheric cusp, *Ann. Geophys.*, 22, 2431–2440, <https://doi.org/10.5194/angeo-22-2431-2004>, 2004.
- Yordanova, E., Vaivads, A., André, M., Buchert, S. C., and Vörös, Z.: Magnetosheath Plasma Turbulence and Its Spatiotemporal Evolution as Observed by the Cluster Spacecraft, *Phys. Rev. Lett.*, 100, 205003, <https://doi.org/10.1103/PhysRevLett.100.205003>, 2008.
- 20 Yordanova, E., Balogh, A., Noullez, A., and von Steiger, R.: Turbulence and intermittency in the heliospheric magnetic field in fast and slow solar wind, *J. Geophys. Res.-Space*, 114, A08101, <https://doi.org/10.1029/2009JA014067>, 2009.
- Zhang, J., Richardson, I. G., Webb, D. F., Gopalswamy, N., Huttunen, E., Kasper, J. C., Nitta, N. V., Poomvises, W., Thompson, B. J., Wu, C.-C., Yashiro, S., and Zhukov, A. N.: Solar and interplanetary sources of major geomagnetic storms ($Dst < -100$ nT) during 1996-2005, *J. Geophys. Res.-Space*, 112, A10102, <https://doi.org/10.1029/2007JA012321>, 2007.
- 25 Zhou, Z., Zuo, P., Feng, X., Wang, Y., Jiang, C., and Song, X.: Intermittencies and Local Heating in Magnetic Cloud Boundary Layers, *Sol. Phys.*, 294, 149, <https://doi.org/10.1007/s11207-019-1537-0>, 2019.

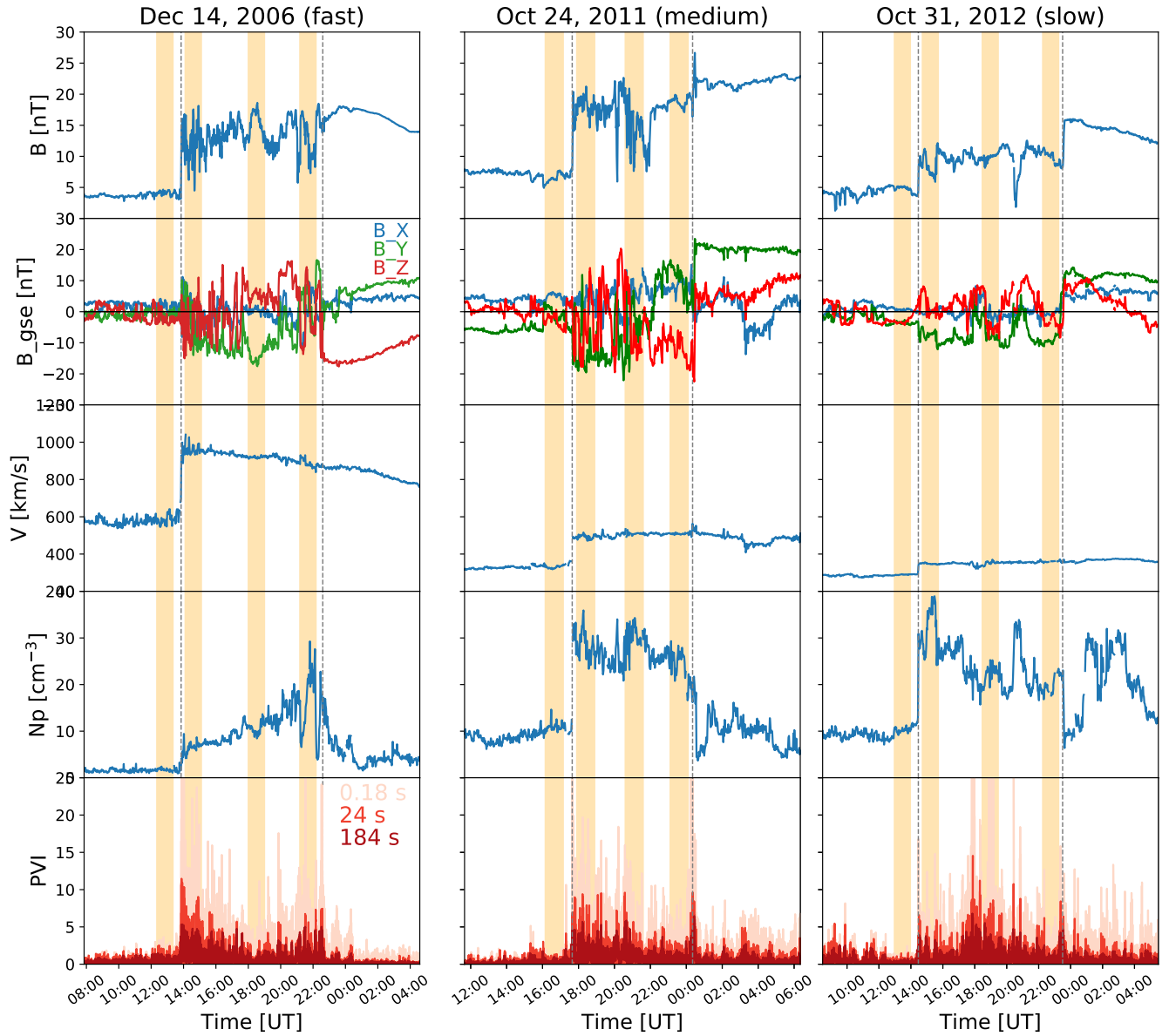


Figure 1. Interplanetary magnetic field and plasma parameters measured at Wind near L1 for the three analysed events. The panels give the a) magnetic field magnitude, b) magnetic field components in GSE coordinates (blue: B_X , green: B_Y , red: B_Z), c) solar wind speed, d) density, and e) PVI-values calculated for 0.18, 24, and 184 seconds (see text for definition). The orange shaded regions show the 1-hour region in the preceding solar wind and those representing three different parts of the sheath: Near-Shock, Mid-Sheath, and Near-LE regions.

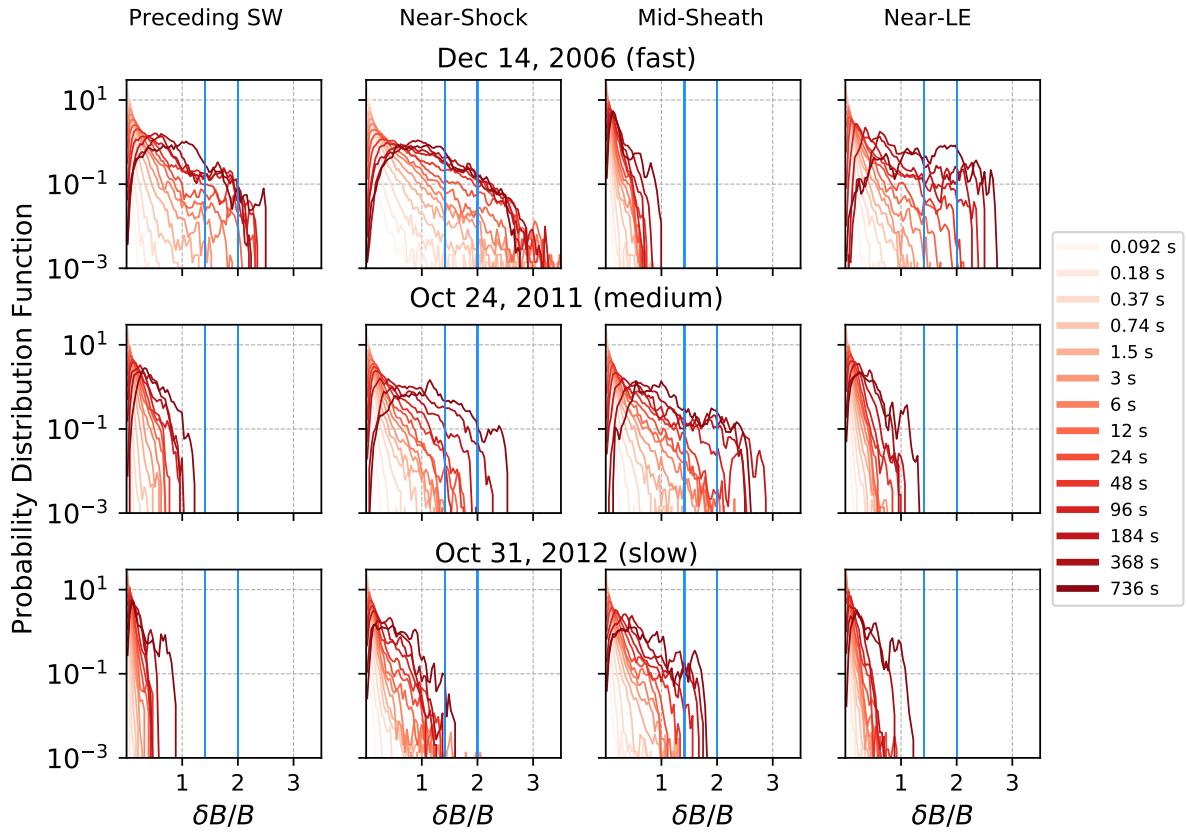


Figure 2. Probability distribution functions of $\delta B/B$ for different timescale Δt (shown as curves of different colours) for Top) December 14, 2006, Middle) October 24, 2011, and Bottom) October 31, 2012 events. The leftmost columns give the results for the solar wind preceding the shock and the following three columns for three different sheath subregions.

Sheath (circle) and preceding solar wind (cross), 1 h

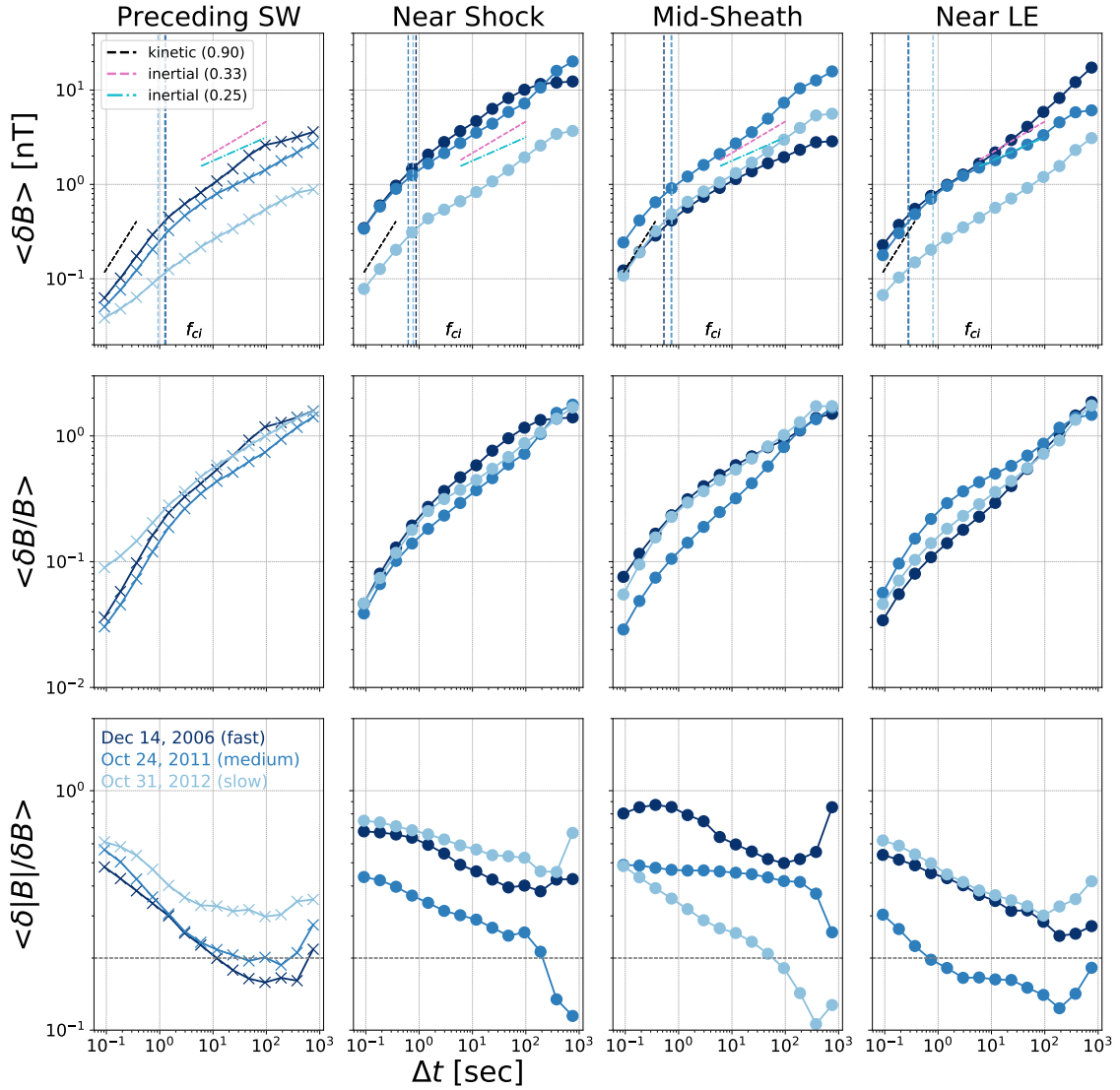


Figure 3. Means of fluctuation amplitudes, $\langle \delta B \rangle$, normalized fluctuations, $\langle \delta B/B \rangle$, and fluctuation compressibility, $\langle \delta|B|/\delta B \rangle$, as functions of timescale Δt . Results are shown separately for the preceding solar wind (crosses) and three different regions of the sheaths (circles). Different colours represent fast (dark blue), intermediate-speed (medium blue), and slow (light blue) sheaths. The dashed vertical lines show the ion cyclotron scales calculated using the magnetic field magnitude averaged over the region in question.

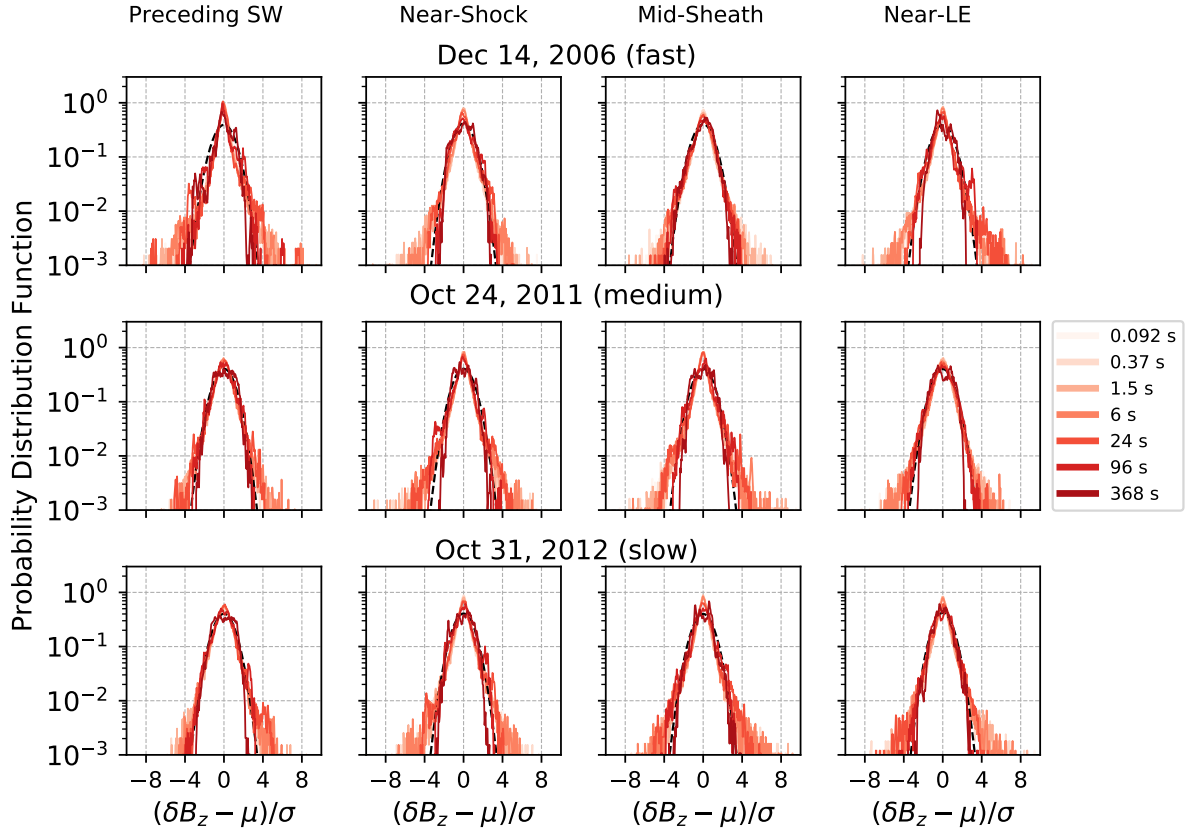


Figure 4. Probability distribution functions of $(\delta B_z - \mu)/\sigma$ (where μ is the average and σ is the standard deviation of δB_z calculated over a 15-minute sliding window) for different timescales Δt (shown as curves of different colours) for Top) December 14, 2006, Middle) October 24, 2011, and Bottom) October 31, 2012 events. The leftmost columns give the results for the solar wind preceding the shock and the following three columns for three different sheath subregions. The black dashed line shows the Gaussian for 6 s timescale.

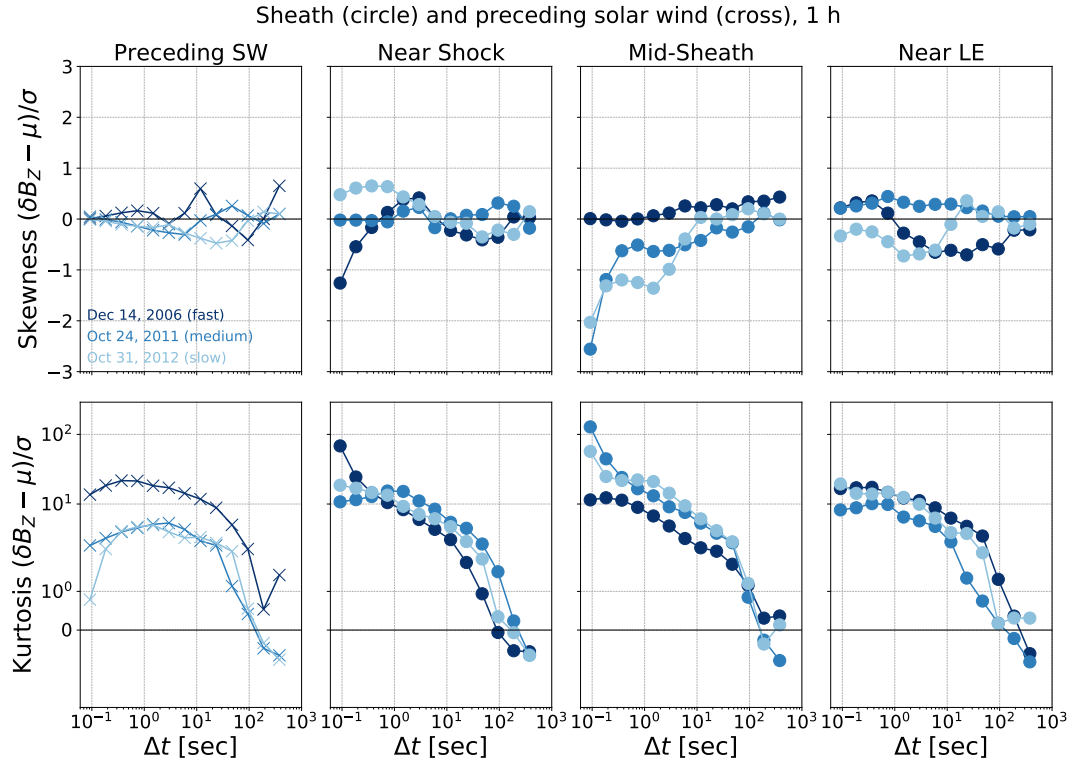


Figure 5. Top) Skewness and Bottom) kurtosis calculated for δB_z as a function of timescale Δt . Different colours and panels represent the fast (dark blue), intermediate-speed (medium blue), and slow (light blue) sheaths. The dots indicate the values in the sheath and the crosses in the preceding solar wind.

Scaling exponent $g(m)$ vs. moment m , p -model

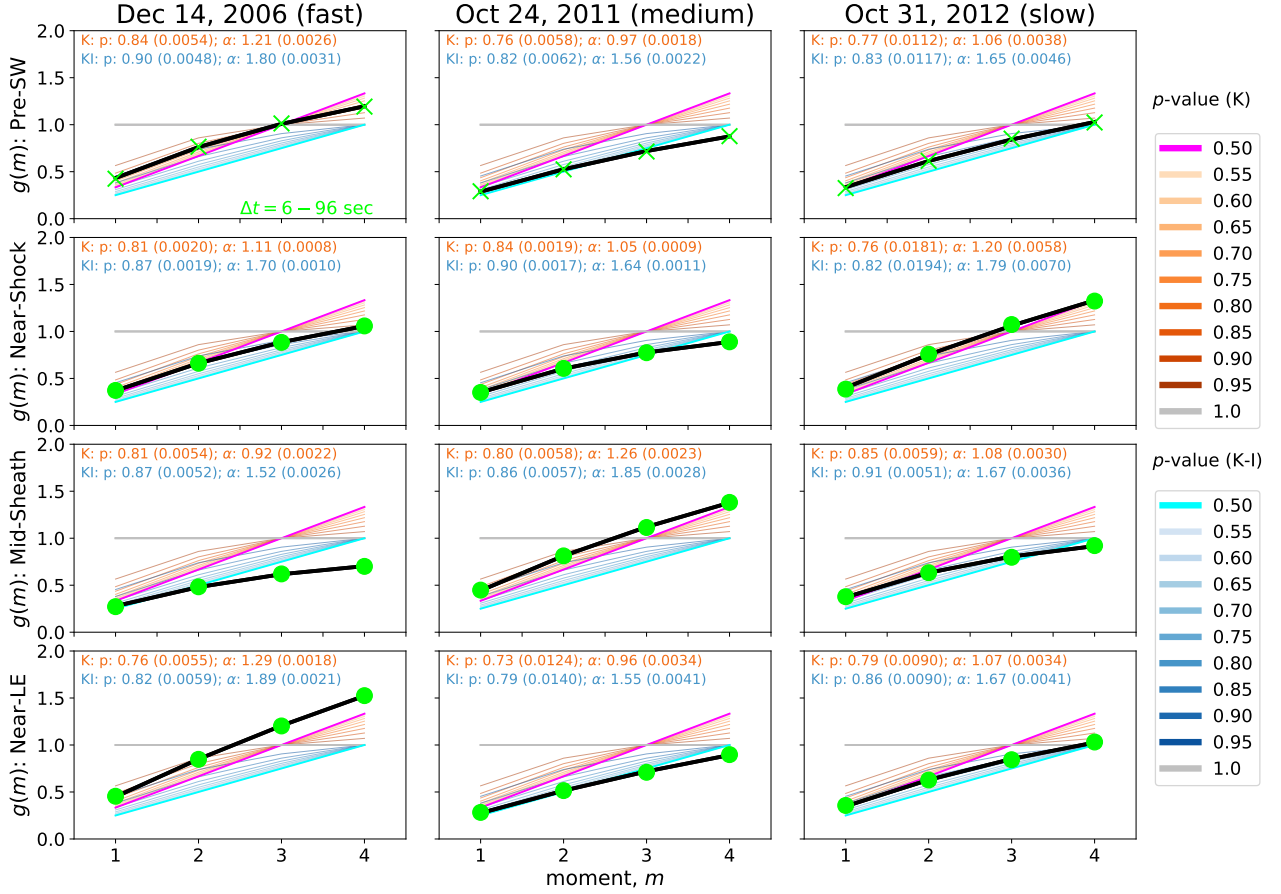


Figure 6. The dots and crosses show the scaling exponent $g(m)$ for the structure function $\langle |B(t + \Delta t) - B(t)|^m \rangle$ as a function of moment m (m is set to range from 1 to 4) for the preceding solar wind and three subregions of the sheath. The orange and blue curves show the results for the standard p -model with p ranging from 0.5 to 1 in steps of 0.05 for the Kolmogorov's (K) and Kraichnan–Iroshnikov (K–I) forms, respectively. The non-intermittent cases ($p = 0.5$) are shown by pink (K) and cyan (K–I), while the grey horizontal curve gives the maximum intermittency case ($p = 1$). The bright green dots show the results calculated for timescales $\Delta t = 6\text{--}96$ s, corresponding to the inertial range. The thick black line shows the least square fits for the extended p -model. The values show the values of p and α parameters for the Kolmogorov's (orange) and Kraichnan–Iroshnikov (blue) forms with standard deviation errors in parenthesis.